HIGH SPIN STATES AND NEUTRON MULTIPLICITIES AFTER PION CAPTURE IN ^{181}Ta AND ^{209}Bi

R. Beetz, F.W.N. de Boer*) and J.K. Panman,
Institute of Nuclear Physics Research, Amsterdam,
The Netherlands

J. Konijn**), P. Pavlopoulos, G. Tibell and K. Zioutas,
CERN, Geneva, Switzerland

I. Bergström and K. Fransson,
Research Institute for Physics, Stockholm, Sweden

G. Backenstoss and L. Tauscher,
Institute of Physics, University of Basle, Basle, Switzerland

P. Blüm, R. Guigas, H. Koch, H. Poth and L.M. Simons,
Kernforschungszentrum und Universität Karlsruhe,
Institut für Kernphysik, Karlsruhe, Germany

ABSTRACT

The absorption of stopped π^- in ^{181}Ta and ^{209}Bi has been investigated by studying prompt and delayed γ-ray spectra. Absolute cross-sections for the yield of isotopes per captured π^- in (π^-,xn) reactions, as well as the relative probability of populating nuclear states of different spins have been measured for the hafnium and lead isotopes, respectively. A spin as high as 20 has been observed in the production of ^{204}Pb. The ground-state rotational bands of the hafnium isotopes are excited to spin values up to 16. Neutron multiplicities as large as 15 have been observed for both targets. A neutron multiplicity of $\simeq 8$ is most probable for both tantalum and bismuth targets.

The strong interaction monopole energy shift ε_0 and width Γ_0 for the 4f level are found to be $\varepsilon_0(^{181}\text{Ta}) = 540 \pm 100$ eV; $\varepsilon_0(^{209}\text{Bi}) = 1790 \pm 150$ eV; $\Gamma_0(^{181}\text{Ta}) = 225 \pm 57$ eV; $\Gamma_0(^{209}\text{Bi}) = 1166 \pm 70$ eV. The quadrupole moments, determined from the hyperfine splitting of the 4f pionic atom level, are $Q = 3.30 \pm 0.06$ b and $Q = -0.50 \pm 0.08$ b for ^{181}Ta and ^{209}Bi, respectively.

Geneva - 21 December 1977

(Submitted to Z. Phys.)

---

*) Present address: Natuurkundig Laboratorium der Vrÿe Universiteit, Amsterdam.

**) On leave from the Institute of Nuclear Physics Research, Amsterdam.

1. INTRODUCTION

Many experiments have been performed to look into what happens in heavy nuclei after pion capture [1-12]. It is generally accepted that pion capture on nucleon pairs dominates [13]. The pion rest mass is then equally shared between two nucleons (neglecting binding effects). If the absorption takes place in the nuclear surface region, one of the nucleons is likely to escape the nucleus, which may result in a large nuclear angular momentum change. The other nucleon, when captured by the nucleus, causes a considerable nuclear excitation followed by the evaporation of nucleons, predominantly neutrons [5] with a maximum number of about 8-9. If the absorption takes place in the interior of the nucleus the emission of a larger number of evaporation neutrons is possible (maximum number $\sim$ 17, see [6,14]). In this case, however, the angular momentum should be smaller. Two observables relevant to these features of the pion capture process are thus the number of emitted neutrons x (neutron multiplicity) in a (π^-,xn) reaction and the nuclear angular momentum I. In addition the relative probability of pion capture on *np* pairs relative to that on *pp* pairs or heavier clusters can be studied by measuring the *total yield* of isotopes with an atomic number one unit lower than that of the target nucleus.

Recently, experimental groups at Dubna [2] and SIN [5] reported that nuclear states with high spins were populated in pion capture. The Dubna experiment, using activation techniques, showed, for example, that a high-spin isomer with I = 37/2 in ^{177}Hf was produced in the ^{181}Ta$(\pi^-,4n)$ reaction. This group also reported [6] that up to 16 neutrons were emitted in a ^{201}Hg(π^-,xn) reaction. The SIN group studied prompt gamma-ray spectra following pion capture in ^{165}Ho and ^{175}Lu isotopes [5]. In these experiments it was shown that the maximum cross-section occurred at x = 4 and 5, respectively, and that the rotational spectra were excited up to 12^+ for different Dy and Yb isotopes.

The above results suggest that pion capture could be a convenient way of producing high-spin states in nuclei far off the stability line. In order to investigate the population of high-spin states and neutron multiplicities, we measured the γ-ray spectra of the produced isotopes. In contrast to earlier experiments we recorded the prompt as well as the delayed γ-ray spectra and the long-lived activation produced. As targets we selected one spherical (^{209}Bi) and one deformed (^{181}Ta) nucleus. The reason for choosing these particular nuclei was the fact that high-spin states are fairly well known in a wide region of isotopes of Pb and Hf.

2. EXPERIMENTAL TECHNIQUES

The experiment was performed at the CERN Synchro-cyclotron (SC) muon channel, using pions of an energy of 125 MeV. The circular beam spot on the target had a diameter of about 10 cm. In order to slow down the pions, we used a graphite degrader.

Two different targets were used in the experiment:

i) a Ta target consisting of two plates (each 2.49 g/cm^2 thick) of metallic tantalum of about 14 cm × 10 cm, constructed in the shape of a cross, and

ii) a Bi powder-target (1.22 g/cm^2) contained in a thin plastic cover of the same shape and dimensions as the other target.

A stopped pion was defined by a combination of four scintillation counters and a Čerenkov counter (see Fig. 1). The number of stopped particles per second was about 5×10^4. Two Ge(Li) detector systems were used, both viewing the target at angles perpendicular to the direction of the incident beam. On one side of the target, at a distance of 16 cm, a semi-planar 15 cm^3 Ge(Li) detector (efficiency 2% at 1.3 MeV) was used, and on the opposite side, 32 cm from the target, a closed-end Ge(Li) detector (efficiency 10% at 1.3 MeV), mounted in a Compton suppression device [15]. The NaI(Tl) crystal (Ø = 25.4 cm; L = 25.4 cm) of this latter system was shielded by a cylinder of 5 cm of lead. Another 5 cm of lead was placed between this cylinder and the target.

The experimental set-up was arranged in the same way for both targets, choosing three different time windows:

time window 1: (prompt) recorded γ-rays emitted up to 50 nsec after a π^- stop.

time window 2: (delayed 1) recorded γ-rays from 50 nsec up to 1 μsec after a π^- stop.

time window 3: (delayed 2) recorded γ-rays from 1 μsec up to the next π^- stop.

The spectra were measured in 2048 channels. For the large diode the selected energy range extended up to 2 MeV, and for the semi-planar detector up to about 1 MeV.

In order to correct for γ-rays resulting from the muon contamination in the pion beam, spectra were collected for a stopped muon beam on the Bi target. Furthermore, the radioactivity of the targets was measured, immediately after the pion irradiations.

The efficiency of the detectors was calibrated with a set of absolutely calibrated sources. Because of the rather thick targets self-absorption in the targets was taken into account in the evaluation. Minor corrections of the

detection efficiency had to be applied for losses in the fast Ge(Li)-telescope coincidences owing to the limited time resolution of the detectors.

For energy calibration, several well-established nuclear γ-ray transitions occurring in the spectra were used. In addition, transitions produced in the background $(n,n'\gamma)$ reactions in ^{19}F, ^{23}Na, ^{127}I [from the surrounding NaI(Tl) crystal], ^{27}Al (from the detector cap), and some Pb-lines from the lead shield could be used. These lines were observed in all three time gates. The main background lines are listed elsewhere [15]. Additional calibration energies are available from the pionic X-ray transitions in the prompt spectra, where one can use the calculated electromagnetic energy values of the levels with $n \geq 5$.

Special care was taken to determine the background lines produced in all kinds of reactions in the surrounding material. In the Compton-suppressed spectra most of these lines are transitions in ^{127}I and in the stable Pb isotopes, present in the shielding. Relative neutron fluxes during the three time intervals were determined from the intensities of several transitions in ^{127}I. Integrated neutron flux ratios of 1.0:0.7:8.0 were observed for the three time intervals, corresponding to the time windows of 50 nsec, 0.95 μsec and about 10 μsec, respectively. These figures show that the prompt neutron flux (during the prompt time window) is much higher than the delayed ones.

Since the time windows were kept identical for both targets, it was possible to determine the background contamination in any spectrum, Ta or Bi, by comparing that spectrum with all the others. In particular, γ-rays due to inelastic neutron scattering in the Pb shield of the Compton-suppressed Ge(Li) detector showed up clearly in the Ta measurement and were used for correcting the Bi measurement. Furthermore, background lines in the spectra from the Compton-suppressed Ge(Li) detector could be subtracted by comparison with the spectra from the semi-planar one, as the small detector is not disturbed by background lines from the NaI(Tl) crystal. The evaluation of the generally weak nuclear γ-rays of interest was difficult and partly impossible in the prompt neutron-induced and pionic X-ray background. These difficulties are not present in the delayed spectra. Figures 2 to 6 show a characteristic set of measured gamma-ray spectra.

3. EXPERIMENTAL RESULTS

3.1 The pionic X-rays

The pionic X-rays of ^{209}Bi and ^{181}Ta are seen in the prompt spectra shown in Figs. 2, 4, and 5. Because of nuclear capture by the strong interaction, the pions almost never reach orbits with $n < 4$ and $\ell < 3$. The X-ray transition to the last level therefore exhibits the usual features of a strong interaction induced energy shift ε_0 and a line broadening Γ_0, as well as a pionic X-ray hyperfine pattern for our target nuclei.

Shifts

From the energy calibration, as described in Section 2, we determine the energies of the 5g → 4f and 6g → 4f transitions in ^{209}Bi and ^{181}Ta. The ε_0(4f) is then derived from a comparison between the calculated values for these transitions and the experimentally determined centre of gravity of the hyperfine pattern (see Table 1 and Refs. 16 and 17).

Widths

In the data analysis of the hfs the experimental Gaussian line shape is folded with a Lorentzian one, representing the natural width of the line. The instrumental resolution was obtained as described in Ref. 18. The measured pionic X-ray Lorentzian line shapes gave Γ_{exp}(Ta) = 328 ± 57 eV and Γ_{exp}(Bi) = 1329 ± 70 eV. Taking the electromagnetic broadening of the 4f level (see Table 1) into account, one obtains values for Γ_0 (see Table 1) which are in good agreement with earlier reported values [19]. The electromagnetic broadening of the 5g level has to be subtracted in a different way (quadratically) and is therefore negligible. The resulting values for Γ_0 and ε_0 for the pionic 4f level agree well with general systematics of the 4f level [20].

Quadrupole moments

For a detailed description of the formalism and analysis of the experimental data of the effective quadrupole moment, the reader is referred to our already published analysis of ^{181}Ta [18].

Since the ^{209}Bi nucleus is almost spherical, it has a very small spectroscopic quadrupole moment Q. However, owing to the rather large ground-state spin $I = 9/2$ of ^{209}Bi the hyperfine splitting of the 4f level could be determined. This was done in a similar way as is described in Ref. 18 and in the following we use the notations defined there. The correction for the magnetic hfs was applied using interaction constants A_1 of 5.719 eV and 1.366 eV for the 4f and 5g levels, respectively. The electric quadrupole interaction constants A_2^P were calculated to be 737.2 eV/b and 188.2 eV/b for the above-mentioned levels, respectively. Using these interaction constants an effective quadrupole moment Q_{eff}(Bi) = -0.53 ± 0.09 b was determined from the energy splitting ΔE = -447 ± 76 eV between the $^{17}/_2 \rightarrow {}^{15}/_2$ and the $^{15}/_2 \rightarrow {}^{13}/_2$ members of the 5g → 4f pionic X-ray hf complex. The finite size corrections were calculated to be 1.1% for ^{209}Bi, whereas ε_2, the strong interaction quadrupole shift, was calculated from the experimental value for ε_0(4f) (see Table 1) and the theoretically calculated ratio $\varepsilon_2/\varepsilon_0$ = -0.018 assuming the ^{209}Bi nucleus to have a β_2 of approximately -0.02. The spectroscopic quadrupole moment, corrected for the strong interaction, is then Q = -0.50 ± 0.08 b as obtained from pionic ^{209}Bi. In Table 2 our experimental result is listed together with earlier reported values [21-28].

The final results on the ^{181}Ta quadrupole moments [see Ref. 18] are Q_{eff}(Ta) = 3.58 ± 0.03 b and for the spectroscopic quadrupole moment Q = 3.30 ± 0.06 b (see Table 1).

3.2 Nuclear γ-ray transitions

The population of levels in different lead isotopes with A = 207 - 194 produced in ^{209}Bi$(\pi^-,xn)^{(209-x)}$Pb reactions as well as hafnium isotopes with A = 179 - 166 in the ^{181}Ta$(\pi^-,xn)^{(181-x)}$Hf reactions has been determined by comparing energies and intensities of the various γ-ray transitions with the decay properties of these isotopes. The isotopic yield per stopped pion was obtained by normalizing the experimental γ-ray intensities to the calculated pionic X-ray intensities (see Section 4.1). The results are presented in Tables 3 and 4 and in Figs. 7 to 15. In these figures we have plotted yields as a function of neutron multiplicity or nuclear spin.

The experimental results illustrated by Figs. 7 to 11 can be summarized as follows:

i) The total yield of all pion capture processes leading to isotopes in Pb and Hf are found to be 0.74 ± 0.07 and 0.79 ± 0.06, respectively.

ii) The average multiplicity of neutrons emitted is 7.9 and 7.5 for ^{181}Ta and ^{209}Bi, respectively (see Figs. 7 and 8).

iii) A neutron multiplicity as high as 15 is observed for both targets (see Figs. 7 and 8 and Tables 3 and 4).

iv) The yield for x = 13 in Hf and x = 15 in Pb is as high as 5% of the maximum isotopic yield, corresponding to about 0.8% of the total yield given above [see (i)].

v) The half width of the isotopic yield curve is ≃ 5 for Hf and 8 for Pb.

vi) The yield curve is almost symmetric for Hf but asymmetric for Pb (possibly indicating an overlap of two unresolved bell shaped curves).

vii) In Hf isotopes high-spin states (14-16) are populated with about the same yield independent of the multiplicity (see Figs. 9 and 10).

viii) The γ-ray yield as a function of spin of the initial state decreases exponentially in the case of the Hf isotopes. This seems also to be the case for the lighter Pb isotopes up to A = 203 for spins up to I = 10.

ix) In the population of high-spin states relative to that of low-spin states in Hf isotopes there is a minimum for intermediate multiplicities (see Fig. 11). This is not the case for the lead isotopes.

x) The largest angular momentum observed is I = 20 for ^{204}Pb (x = 5).

xi) There seems to be a particularly enhanced population of I = 9 and I = 17 states in ^{204}Pb.

4. DISCUSSION

4.1 The pionic cascade

The pion cascade has to be discussed in order to find out from which ℓ state the π^- is captured predominantly. We assume the initial population and the cascade mechanism to be the same as for muons [13] except for the initial main quantum number now being n = 20. In addition, we introduce the measured absorption width into the cascade and scale it for other n, ℓ states.

A cascade program based on these assumptions shows that ≃ 90% of the pion transitions populate the 4f level.

4.2 Pion absorption in the nucleus

Because of conservation of momentum and energy, the pion cannot be absorbed on a free nucleon and experiments have shown [7] that absorption on one nucleon is a rare process also in nuclei.

Conservation of charge restricts the two-nucleon absorption to *np* and *pp* pairs corresponding to the processes

$$\pi^- + np \rightarrow n + n \qquad \text{(a)}$$

$$\pi^- + pp \rightarrow n + p \ . \qquad \text{(b)}$$

Process (a) should lead to Pb and Hf isotopes, respectively, with the two targets used. Regarding process (b), there should be about equal chances for the proton and neutron to leave the nucleus because the Coulomb barrier (∿ 14 MeV) is small compared to the kinetic energy of the proton (∿ 70 MeV).

If the probability of pion capture only depends on the concentration of nucleon pairs, the fraction of *np* capture processes is

$$P_{np} = \frac{N \cdot Z}{NZ + \frac{1}{2} Z(Z - 1)} \ ,$$

an expression which has a value of about 0.76 for heavy nuclei. The corresponding fraction P_{pp} is thus 0.24. Hence, the yield per stopped pion of Pb and Hf isotopes should be about 0.76 + 1/2 · 0.24 = 0.88 and the yield of Tl and Lu isotopes should be about 0.12, neglecting pion absorption on three, four, or more nucleons.

However, after heating the nucleus the probability of producing a $[\pi^-, p(x-1)n]$ reaction is about 15% of that of producing a (π^-, xn) one. Introducing this correction, we find that the expected yield 0.88 for process (a) mentioned above should be reduced to ∿ 0.75. It is now interesting to find that the experimental yields of Pb and Hf isotopes are 0.74 ± 0.07 and 0.79 ± 0.06, respectively.

We therefore conclude that the capture on *np* pairs dominates in heavy nuclei corresponding to the fact that *np* pairs are more frequent than *pp* pairs. Our data, however, do not allow for any statement about capture on preformed clusters.

4.3 Neutron multiplicity and angular momentum

Nuclear de-excitation and neutron multiplicity have been dealt with by a number of authors like, for example, Locher and Myhrer [29], Gadioli et al. [30] and Iljinov et al. [31]. In order to be able to compare our experimental results with the semi-empirical calculations of these authors and with our own calculations, we first briefly discuss some possible modes of pion absorption.

In Fig. 12 two extreme positions are indicated for pion absorption, namely the surface *(case a)* and the interior *(case b)* of the nucleus.

In case a, where the pion is absorbed on a *nucleon pair in the nuclear surface*, one nucleon leaves the nucleus with an energy of about 70 MeV, whereas the other starts a multiple scattering process, exciting it to about 70 MeV. Subsequently, the de-excitation will occur by evaporation of thermalized neutrons; a process with a maximum neutron multiplicity of about 8, since the average neutron binding energy is about 8 MeV [14]. Our measurements show (see Section 3.2) that the *average* neutron multiplicity is 7 to 8, indicating that an appreciable amount of absorption in heavy nuclei does not occur in the nuclear surface.

The fast neutron, in leaving the nucleus, forces it to twist around, a process which can be considered to be the opposite effect to the introduction of angular momentum by fast particle reactions. A 70 MeV ($p \simeq 370$ MeV/c) neutron leaving a lead nucleus tangentially introduces a maximum angular momentum $L_0 = R \times p$ of about $16\hbar$, assuming the nucleus to be a uniformly dense sphere of radius R. (In the Ta case the L_0 value is smeared out by about $4\hbar$ owing to the deformation of the nucleus, $\beta_2 = 0.265$.) In the case of neutron multiplicity $x = 7$ one would then expect low angular momenta.

The average angular momentum $\bar{L}$ in the case of isotropic neutron emission is related to the maximum possible angular momentum L_0 by

$$\bar{L} = \frac{\pi}{4} L_0 \ .$$

This gives values for $\bar{L}$ of $11.6\hbar$ and $12.1\hbar$ for ^{181}Ta and ^{209}Bi, respectively. To get the total spin, we must add the angular momentum F, composed of the initial target spin and the angular momentum of the pion ℓ_π at the moment of capture. This leads to average F values of $\langle F \rangle = 9/2$ and $\langle F \rangle = 11/2$ for ^{181}Ta and ^{209}Bi, respectively, as observed in the hf pattern of the $5 \rightarrow 4$ X-ray transitions. From this simple argumentation, average angular momenta of residual nuclei of about 13 are obtained, in disagreement with our observations.

By also including into our considerations the Fermi momentum of the pion absorbing nucleon pairs, the maximum observable angular momentum in our nuclei could therefore be as high as 25$\hbar$. The maximum spin observed in this experiment is I = 20 in ^{204}Pb.

We conclude that *case a* alone cannot be responsible for the absorption of the π^-.

In case b (Fig. 12) the absorption on a *nucleon pair* takes place so *far inside the nucleus* that both nucleons are absorbed. The maximum value x = 15 to 16 found in this work and other investigations is a consequence of a simple energy balance of the pion absorption in the interior of the nucleus. The (π^-,15n) reactions in ^{181}Ta and ^{209}Bi have Q values of 22.5 MeV and 24.6 MeV, respectively (see also Table 5). These extreme cases of pion absorption in the interior of the nucleus should therefore give rise to 15 evaporation neutrons with an average kinetic energy of 1 to 2 MeV. Hence, the maximum value of the neutron multiplicity x is set by the pion rest mass and the Q values of the (π^-,xn) reactions.

The evaporation neutrons in *case b*, being randomly emitted, should not induce very high angular momenta. One therefore would not expect population of high angular momenta in Pb and Hf nuclei together with high neutron multiplicities (x > 10).

This is, however, not confirmed by our measurements, at least not in the case of Ta, where the ratio of production of high-spin states relative to that of low-spin states increases with neutron multiplicity for x > 7 (see Fig. 11).

Returning to the semi-empirical calculations mentioned at the beginning of this section, we take the work of Iljinov et al. [31] as a basis for our discussion. They use the so-called intranuclear cascade model for calculating the energy dissipation after pion absorption and add Fermi motion to the nucleons. For the neutron energy distribution these authors find a narrow low-energy peak (a few MeV broad) corresponding to evaporation neutrons (essentially *case b*) and a broad bump at about 55 MeV, corresponding to fast neutrons due to events mainly in the nuclear surface (*case a*). They also calculate the multiplicity distribution and find a maximum yield at x = 7 for absorption on a nucleon pair. Absorption on a *quasi-alpha* particle leads to a very asymmetric yield distribution with a maximum at x = 11. It thus seems that our experimental yield with a maximum at x = 8 confirms that π^- absorption on a nucleon pair dominates entirely in the case of a ^{181}Ta target. In the case of ^{209}Bi there is a slight yield excess for high x values, which in the model of Iljinov et al. [31] could be due to an absorption on *quasi-alpha* particles.

It should be pointed out that our yield measurements disagree with the calculations of Iljinov et al. [31] for very low neutron multiplicities ($x < 3$). The calculations by Gadioli et al. [30] give qualitatively similar results. In the particular region of small x their results are in better agreement with our results (see Fig. 7). Their calculations for Ta, however, do not reproduce the narrow multiplicity distribution of this experiment (Fig. 8).

Also Locher and Myhrer [29] obtain results for the neutron multiplicity in agreement with earlier experimental results [5]. They work with a model for the absorption which resembles *case a* above, using experimental data for the nucleon emission spectrum and cross-sections for (p,xn) reactions.

Calculations of the angular momentum of the residual nucleus have been carried out [31]. The probability distribution obtained has a maximum for spins 4 to 5 and drops down almost linearly to zero for a spin of 17. It should be pointed out, however, that nuclear spins and the pion angular momentum have been neglected in this calculation. This prediction is at variance with our observation which shows highest probability for lowest angular momenta and an exponential decrease for high I.

In the following we try to relate the (π^-,xn) reaction, as far as angular momentum distributions are concerned, to conventional nuclear reactions resembling the π absorption most. Therefore, we have calculated for the (n,xn) reaction, with x ranging from 2 to 10, the statistical angular momentum distribution before γ emission, using a slightly modified version of the optical model calculations described by Lindén et al. [32]. As a result we obtain a distribution with an asymmetric bell shape. Taking the ^{179}Hf(n,6n)^{174}Hf reaction as an example, the maximum cross-section occurs for spins 5 and 6 with a direct population of the ground state as well as the I = 15 state of about 1% of the maximum yield. To compare this calculated distribution with experimental data on gamma intensities, we have to integrate the calculated curve above the spin value of interest. Such comparisons are shown in Figs. 13-15 where in some cases we have averaged the calculated yields over three incident neutron energies, in steps of 10 MeV. This averaging is done to simulate the energy distribution of the neutrons produced in the primary pion capture process.

In Fig. 13 we show calculated data for the ^{179}Hf(n,6n)^{174}Hf reaction compared to experimental data on the (π^-,7n) and (π^-,9n) reactions in ^{181}Ta.

In Figs. 14 and 15 we show similar plots for the ^{209}Bi data. The (π^-,xn) experimental results do not seem to be in agreement with our calculations for any values of x. Evidently, the (π^-,xn) reactions have more specific features which are not reproduced in (n,xn) and (α,xn) calculations.

5. CONCLUDING REMARKS

Some of the observations listed in Section 3.2 can be explained in terms of a relatively simple model for the pion absorption mechanism and subsequent nuclear processes. The bulk of the absorption seems to occur on nucleon pairs, preferably on *np* pairs.

As far as neutron multiplicities are concerned, we remark:

The average neutron multiplicity is reproduced by all calculations based on a two-nucleon absorption mechanism, implying that it is not particularly sensitive to details of the energy dissipation in the nucleus.

Shapes of multiplicity distributions are more sensitive to absorption mechanisms. In particular for low multiplicities the calculations differ. At high multiplicities the nuclei Ta and Bi differ significantly inasmuch as Bi shows an enhancement for high x. This is tentatively ascribed to additional absorption on α clusters in Bi, which would be absent in Ta.

Very low ($x \leq 3$) and very high ($x \geq 13$) multiplicities are equally improbable.

Concerning the high spin states we remark: the observed maximum angular momentum is compatible with simple kinematical considerations. The average spin induced is about I = 6 in Ta, corresponding to a spin of about 4 introduced by the absorption mechanism alone, regarding the fact that absorption takes place from $\langle F \rangle = {}^{9}/_{2}$ states mainly. The population of high spin states is enhanced for low multiplicities ($x < 7$), as qualitatively expected from simple kinematics. It decreases for increasing multiplicities, according to the fact that for such multiplicities no sufficiently fast neutrons are available for inducing high L values. In the case of Ta, however, the population of high spin states is again enhanced, when going to multiplicities higher than $x = 7$. Spins as high as 16 are populated in Hf even for multiplicities $x = 14$. This phenomenon is not understood.

Whereas for Ta the population of spins decreases exponentially with increasing spin, this is not true for all multiplicities in Bi. In particular ^{204}Pb shows a pronounced rupture of spin population at I = 9. In fact it seems as if mainly I = 9 and I = 17 states were populated. The population of very high spins in other isotopes unfortunately could not be studied sufficiently in detail.

It is obvious from these points that, although many observations may be explained by simple considerations, there are other features which contain more information since they require a more detailed knowledge of the absorption mechanism and of the actual structure of the nucleus to be explained.

It may finally be remarked that with pion absorption one reaches a high nuclear excitation (up to 140 MeV) and that the introduction of a negative charge leads to residual nuclei, which may not be so easy to produce in other reactions.

This work is part of the research program of the Institute for Nuclear Physics Research (IKO) made possible by financial support from the Foundation for Fundamental Research on Matter (FOM) and the Netherlands Organization for the Advancement of Pure Research (ZWO).

REFERENCES

[1] M.E. Nordberg, K.F. Kinsey and R.L. Burman, Phys. Rev. 165 (1968) 1096.

[2] V.S. Butsev, Ya. Vandlik, Ts. Vylov, Dz. Ganzorig, L. Gumnerova, N.G. Zaitseva, S.M. Polikanov and D. Chultem, Yad. Fiz. 23 (1976) 17.

[3] V.S. Butsev, Dz. Ganzorig, S.M. Polikanov and D. Chultem, Abstract submitted to the 25th Meeting on Nuclear Spectroscopy and Structure of the Atomic Nucleus, Leningrad, 1975, p. 150.

[4] V.S. Butsev, Yu.K. Gavrilov, Dz. Ganzorig, S.M. Polikanov and D. Chultem, JETP Letters Sov. Phys. 21 (1975) 400.

[5] P. Ebersold, B. Aas, W. Dey, R. Eichler, H.J. Leisi, W.W. Sapp and H.K. Walter, Phys. Lett. 58B (1975) 428.

[6] V.M. Abazov, S.R. Avramov, V.S. Butsev, E.P. Cherevatenko, D. Chultem, W.D. Fromm, Dz. Ganzorig, Yu.K. Gavrilov and S.M. Polikanov, Nucl. Phys. A274 (1976) 463.

[7] H.D. Engelhardt, C.W. Lewis and H. Ulrich, Nucl. Phys. A258 (1976) 480.

[8] V.S. Butsev, D. Chultem, E.P. Cherevatenko, Yu.K. Gavrilov and S.M. Polikanov, Dubna preprint E15-9825, 1976.

[9] V.S. Butsev, D. Chultem, Yu.K. Gavrilov, Dz. Ganzorig and V. Presperin, Nucl. Phys. A285 (1977) 379.

[10] W. Dey, H.P. Isaak, H.K. Walter, R. Engfer, H. Guyer, R. Hartmann, E.A. Hermes, H. Müller, H.S. Pruys, W. Reichart and J. Morgenstern, Helv. Phys. Acta 49 (1976) 778, and contribution to the Frühjarstagung der Schweizerischen Phys. Gesellschaft, 1977.

[11] S.R. Avramov, V.S. Butsev, D. Chultem, Yu.K. Gavrilov, Dz. Ganzorig and S.M. Polikanov, Proc. VI Internat. Conf. on High Energy Physics and Nuclear Structure, Santa Fe, 1975, p. 190.

[12] H.S. Pruys, R. Hartmann, R. Engfer, U. Sennhauser, W. Dey, H.-J. Pfeiffer, H.K. Walter, J. Morgenstern and A. Wyttenbach, Helv. Phys. Acta 50 (1977) 199.

[13] J. Hüfner, Physics Reports 21C (1975) 1.

[14] 1975 Mass-excess predictions, Atomic Data and Nuclear Data Tables 17 (1976) 477.

[15] R. Beetz, W.L. Posthumus, F.W.N. de Boer, J.L. Maarleveld, A. v.d. Schaaf and J. Konijn, Nucl. Instr. Meth. 145 (1977) 353.

[16] F. Scheck, Nucl. Phys. B42 (1972) 573.

[17] C. Ekström, H. Rubinsztein and P. Möller, Physica Scripta 14 (1976) 199.

[18] R. Beetz, F.W.N. de Boer, K. Fransson, J. Konijn, J.K. Panman, L. Tauscher and G. Tibell, Determination of the effective quadrupole moment in ^{181}Ta with pionic X-rays, to be published in Nucl. Phys.

[19] H. Schmitt, L. Tauscher, G. Backenstoss, S. Charalambus, H. Daniel, H. Koch and G. Poelz, Phys. Lett. 27B (1968) 530.

[20] L. Tauscher, Lectures given at the First Internat. School on Exotic Atoms and Related Topics, Erice, 1977.

[21] L.O. Dickie and F.M. Kelly, Can. Journ. Phys. 45 (1967) 2249.

[22] R.J. Powers and V.L. Telegdi, Z. Physik 202 (1967) 214 and R.J. Powers, Phys. Rev. 169 (1968) 1.

[23] G. Eisele, I. Koniordos, G. Müller and R. Winkler, Phys. Lett. 28B (1968) 256.

[24] D.A. Landman and A. Lurio, Phys. Rev. A1 (1970) 1330.

[25] S. George and R.A. Klingberg, J. Opt. Soc. Am. 60 (1970) 869.

[26] W.Y. Lee, M.Y. Chen, S.C. Cheng, E.R. Macaguo, A.M. Rushton and C.S. Wu, Nucl. Phys. A181 (1972) 14.

[27] A. Rosén, Physica Scripta 6 (1972) 37.

[28] I. Lindgren and A. Rosén, Case Studies in Atomic Physics 4 (1974) 199.

[29] M.P. Locher and F. Myhrer, Helv. Phys. Acta 49 (1976) 123.

[30] E. Gadioli and E. Gadioli-Erba, Nucl. Phys. A256 (1976) 414, and private communication.

[31] A.S. Iljinov, V.I. Nazaruk and S.E. Chigrinov, Nucl. Phys. A268 (1976) 513.

[32] C.G. Lindén, I. Bergström, J. Blomqvist, K.G. Rensfelt, H. Sergolle and K. Westerberg, Z. Phys. A277 (1976) 277.

Table 1

Pionic X-ray data, relevant for the strong interaction effects, such as the monopole shifts, ε_0, and widths, Γ_0. The spectroscopic quadrupole moments Q are deduced from the hf pattern of the 5→4 X-ray transitions in the pionic cascade.

	^{181}Ta		^{209}Pb	
	Experimental values	Calculation without strong interaction	Experimental values	Calculation without strong interaction
Transition energy: 5g → 4f	453.55 ± 0.11 keV	453.020 keV	589.68 ± 0.10 keV	588.028 keV
6g → 4f	696.89 ± 0.23 keV	696.330 keV	904.92 ± 0.11 keV	902.965 keV
The strong interaction monopole width, Γ_0(4f) of the 4f level	225 ± 57 eV		1166 ± 70 eV	
The electromagnetic width Γ_e,				
of the 4f level Γ_e(4f)		79.0 eV		124.4 eV
of the 5g level Γ_e(5g)		24.4 eV		38.4 eV
The strong interaction monopole shift, ε_0(4f)	540 ± 100 eV		1790 ± 150 eV	
Effective quadrupole moment Q_{eff}	3.58 ± 0.03 b		-0.53 ± 0.09 b	
Spectroscopic quadrupole moment Q	3.30 ± 0.06 b	3.25 b *)	-0.50 ± 0.08 b	

*) Calculated for the Nilsson state [404]↓, $7/2^+$ in ^{181}Ta with $\beta_2 = 0.263$ and $\beta_4 = -0.052$ by Ekström et al. [17].

Table 2

Values for the spectroscopic quadrupole moment Q in ^{209}Bi from the present experiment together with previously reported results. The strong interaction correction to $Q_{eff} = -0.53 \pm 0.09$ b is discussed in the text.

Method and year of publication	Spectroscopic quadrupole moment Q in b	Ref.
Optical spectroscopy (1967)	-0.37 ± 0.04	[21]
Muonic atom (1967-1968)	-0.37 ± 0.05	[22]
Optical spectroscopy (1968)	-0.379 ± 0.015	[23]
Atomic beam (1970)	-0.385 ± 0.040	[24]
Optical spectroscopy (1970)	-0.41 ± 0.04	[25]
Muonic atom (1972)	-0.37 ± 0.03	[26]
Theory on optical spectroscopy data (1972-1974)	-0.46	[27,28]
Pionic atom (1977)	-0.50 ± 0.08	This paper

Table 3

Gamma rays observed in $^{209}Bi(\pi^-,xn)^{209-x}Pb$ reactions as analysed from the prompt and delayed X-ray spectra

Isotope	Transition $I_i \rightarrow I_f$	E_γ (keV)	I_γ (per stopped π^-)	Remarks
^{194}Pb	$2^+ \rightarrow 0^+$	964.2	0.0043 ± 0.0012	
	$4^+ \rightarrow 2^+$	575.0	0.0028 ± 0.0012	
	$7^- \rightarrow 5^-$	420.6	0.0057 ± 0.0026	
^{196}Pb	$2^+ \rightarrow 0^+$	1049.1	0.035 ± 0.004	
	$4^+ \rightarrow 2^+$	689.2	0.023 ± 0.004	
	$7^- \rightarrow 5^-$	371.7	0.019 ± 0.003	
	$10^+ \rightarrow 9^-$	337.0	0.0039 ± 0.0014	
^{198}Pb	$2^+ \rightarrow 0^+$	1063.5	0.054 ± 0.008	
	$4^+ \rightarrow 2^+$	562.4	-	At Ge-edge
	$5^- \rightarrow 4^+$	197.6	-	$^{19}F + {}^{71m}Ge$
	$10^+ \rightarrow 9^-$	540.9	0.030 ± 0.004	
^{200}Pb	$2^+ \rightarrow 0^+$	1026.5	0.067 ± 0.005	
	$4^+ \rightarrow 2^+$	462.2	0.071 ± 0.005	
	$5^- \rightarrow 4^+$	419.8	0.052 ± 0.004	
	$7^- \rightarrow 5^-$	245.2	$\lesssim$ 0.061	
	$9^- \rightarrow 7^-$	83.8		Not observed
	$10^+ \rightarrow 9^-$	777	0.017 ± 0.003	
^{202}Pb	$2^+ \rightarrow 0^+$	960.8	0.088 ± 0.013	
	$4^+ \rightarrow 2^+$	422.2	0.094 ± 0.012	
	$5^- \rightarrow 4^+$	657.5	0.050 ± 0.014	
	$9^- \rightarrow 4^+$	786.9	0.029 ± 0.005	
^{202}Tl	$4^- \rightarrow 2^-$	400.4	0.030 ± 0.015	
	$7^+ \rightarrow 4^-$	459.8	0.019 ± 0.005	

Isotope	Transition $I_i \rightarrow I_f$	E_γ (keV)	I_γ (per stopped π^-)	Remarks
^{204}Pb	$2^+ \rightarrow 0^+$	899.15	0.081 ± 0.005	
	$4^+ \rightarrow 2^+$	374.35	0.084 ± 0.011	
	$9^- \rightarrow 4^+$	911.7	0.055 ± 0.018	
	$11^- \rightarrow 9^-$	1005.7	0.014 ± 0.001	
	$12^+ \rightarrow 11^-$	324.7	0.018 ± 0.004	
	$14^+ \rightarrow 12^+$	618.4	0.011 ± 0.002	
	$15^+ \rightarrow 14^+$	167.2	0.015 ± 0.004	
	$16^+ \rightarrow 14^+$	752.9	0.0013 ± 0.0006	
	$16^+ \rightarrow 15^+$	585.7	< 0.004	
	$16^- \rightarrow 15^+$	1046.7	< 0.004	
	$17^- \rightarrow 16^-$	315.9	0.017 ± 0.006	close to π X-ray
	$17^- \rightarrow 16^+$	776.9	0.0026 ± 0.0017	
	$19^- \rightarrow 17^-$	433.7	0.0033 ± 0.0017	
	$20^+ \rightarrow 19^-$	1304.1	0.0036 ± 0.0009	
^{206}Pb	$2^+ \rightarrow 0^+$	803.3	0.038 ± 0.008	Also ^{205}Pb
	$3^+ \rightarrow 2^+$	537.5	0.026 ± 0.003	
	$4^+ \rightarrow 3^+$	343.5	0.022 ± 0.005	
	$4^+ \rightarrow 2^+$	881.0	0.017 ± 0.008	
	$9^- \rightarrow 7^-$	458.1	$\lesssim$ 0.035	
	$10^+ \rightarrow 9^-$	1299.1	0.015 ± 0.004	
^{206}Tl	$2^- \rightarrow 0^-$	265.8	0.0155 ± 0.0016	Also π X-ray
	$4^- \rightarrow 2^-$	686.3	0.0158 ± 0.0016	
	$5^+ \rightarrow 4^-$	453.3	0.015 ± 0.002	Also ^{206}Pb
	$7^+ \rightarrow 5^+$	216.1	0.0181 ± 0.0012	
	$8^+ \rightarrow 7^+$	457.0	0.0039 ± 0.0008	
	$12^- \rightarrow 7^+$	1021.4	0.012 ± 0.002	

Table 3 (cont.)

Isotope	Transition $I_i \rightarrow I_f$	E (keV)	I (per stopped π^-)	Remarks
^{203}Pb gs: $^{5}/_{2}^{-}$	$^{1}/_{2}^{-} \rightarrow$ gs	126.5	0.013 ± 0.012	
	$^{13}/_{2}^{+} \rightarrow$ gs	825.2	0.048 ± 0.004	
	$^{5}/_{2}^{-} \rightarrow$ gs	866.5	0.0037 ± 0.0009	
	$^{5}/_{2}^{-} \rightarrow$ gs	740.1	0.0029 ± 0.0009	
	$^{9}/_{2}^{-} \rightarrow$ gs	896.9	0.0095 ± 0.0012	Also ^{207}Pb
	$^{7}/_{2}^{-} \rightarrow$ gs	933.4	0.0017 ± 0.0008	
	$(^{7}/_{2}, ^{9}/_{2}) \rightarrow$ gs	1198.6	0.0009 ± 0.0008	
	$(^{5}/_{2}, ^{7}/_{2}) \rightarrow$ gs	1203.1	0.0009 ± 0.0008	
	$^{17}/_{2}^{+} \rightarrow ^{13}/_{2}^{+}$	838.7	0.028 ± 0.002	
	$^{21}/_{2}^{+} \rightarrow ^{17}/_{2}^{+}$	258.6	0.028 ± 0.009	
	$\rightarrow ^{21}/_{2}^{+}$	174.0	≤ 0.05	Also ^{71m}Ge
	$\rightarrow ^{21}/_{2}^{+}$	874.0	0.011 ± 0.003	
Total intensity on gs of ^{203}Pb:			0.078 ± 0.013	
^{205}Pb gs: $^{5}/_{2}^{-}$	$^{7}/_{2}^{-} \rightarrow$ gs	703.4	0.0026 ± 0.0008	
	$^{5}/_{2}^{-} \rightarrow ^{1}/_{2}^{-}$	759.2	0.0051 ± 0.0009	
2.23 keV: $^{1}/_{2}^{-}$	$^{7}/_{2}^{-} \rightarrow$ gs	1043.7	≤ 0.009	Also ^{127}I
	$(^{5}/_{2}, ^{7}/_{2}) \rightarrow$ gs	1264.7	0.0033 ± 0.0009	
	$^{13}/_{2}^{-} \rightarrow$ gs	1013.8	≤ 0.018	Also ^{27}Al
	$^{9}/_{2}^{-} \rightarrow ^{7}/_{2}^{-}$ $^{29}/_{2}^{-} \rightarrow ^{29}/_{2}^{-}$	284.1	0.0040 ± 0.0013	
	$^{25}/_{2}^{-} \rightarrow ^{19}/_{2}^{+}$	1175.1	0.0022 ± 0.008	
	$^{21}/_{2}^{-} \rightarrow ^{19}/_{2}^{+}$	1147.4	0.011 ± 0.005	
	$^{21}/_{2}^{+} \rightarrow ^{19}/_{2}^{+}$	534.9	< 0.024	
	$^{19}/_{2}^{+} \rightarrow ^{17}/_{2}^{+}$	323.2	0.020 ± 0.006	Also ^{204}Pb
	$^{17}/_{2}^{+} \rightarrow ^{13}/_{2}^{+}$	683.5	0.020 ± 0.001	
	$^{29}/_{2}^{-} \rightarrow ^{25}/_{2}^{-}$	430.2	0.005 ± 0.002	
Total intensity on gs of ^{205}Pb:			≤ 0.038	
^{207}Pb gs: $^{1}/_{2}^{-}$	$^{5}/_{2}^{-} \rightarrow$ gs	569.7	0.030 ± 0.005	
	$^{3}/_{2}^{-} \rightarrow$ gs	897.3	0.009 ± 0.001	Also ^{203}Pb
	$^{13}/_{2}^{+} \rightarrow ^{5}/_{2}^{-}$	1063.6	0.036 ± 0.005	Also ^{198}Pb
	$^{7}/_{2}^{-} \rightarrow ^{3}/_{2}^{-}$	1434.0	0.004 ± 0.001	
	$^{7}/_{2}^{-} \rightarrow ^{5}/_{2}^{-}$	1769.7	0.004 ± 0.001	
Total intensity on gs of ^{207}Pb:			0.039 ± 0.005	
^{207}Tl gs: $^{1}/_{2}^{-}$	$^{3}/_{2}^{+} \rightarrow$ gs	351.0	≤ 0.028	Also ^{202}Tl
	$(^{11}/_{2}^{-}) \rightarrow ^{3}/_{2}^{+}$	997.0	≤ 0.0025 ± 0.004	

Table 4

Gamma-rays observed in $^{181}Ta(\pi^-,xn)^{181-x}Hf$ reactions, as analysed from the prompt and delayed γ-ray spectra. The yields of the transitions are expressed in units of captured π^-. The normalization is obtained from the intensities of the pionic X-rays.

Transition $I_i \rightarrow I_f$	Hf isotopes						
A:	178	176	174	172	170	168	166
x:	3	5	7	9	11	13	15
$2^+ \rightarrow 0^+$							≤ 0.014
$4^+ \rightarrow 2^+$	0.0156 ± 0.0011	0.054 ± 0.018	0.141 ± 0.010	0.122 ± 0.013	0.0573 ± 0.0030	0.0068 ± 0.0029	-
$6^+ \rightarrow 4^+$	0.0128 ± 0.0020	0.034 ± 0.011	0.0695 ± 0.0041	0.0592 ± 0.0030	0.0289 ± 0.0018	0.0054 ± 0.0025	≤ 0.0067
$8^+ \rightarrow 6^+$	0.0100 ± 0.0006	0.0184 ± 0.0010	0.0287 ± 0.0015	0.028 ± 0.010	0.0208 ± 0.0010	0.0051 ± 0.0023	-
$10^+ \rightarrow 8^+$		0.0122 ± 0.0020	0.0166 ± 0.0018	0.0105 ± 0.0030	0.0121 ± 0.0006	0.0035 ± 0.0005	~ 0.0037
$12^+ \rightarrow 10^+$		0.0078 ± 0.0013	0.0043 ± 0.0012	0.0062 ± 0.0013	-	0.0034 ± 0.0008	≤ 0.0056
$14^+ \rightarrow 12^+$		0.0046 ± 0.0016	0.0041 ± 0.0012	0.0043 ± 0.0003	0.0086 ± 0.0013	0.0028 ± 0.0010	
$16^+ \rightarrow 14^+$					0.0037 ± 0.0004	0.0024 ± 0.0010	

Table 5

Reaction Q-values for (π^-,xn) reactions on ^{181}Ta and ^{209}Bi, respectively, as obtained from the Table 1975 Mass Excess Predictions [14].

Reaction	Q-value (MeV)
$^{209}Bi(\pi^-,18n)^{191}Pb$	-4.1
$^{209}Bi(\pi^-,17n)^{192}Pb$	+6.1
$^{209}Bi(\pi^-,16n)^{193}Pb$	+14.5
$^{209}Bi(\pi^-,15n)^{194}Pb$	+24.6
$^{181}Ta(\pi^-,18n)^{163}Hf$	-7.1
$^{181}Ta(\pi^-,17n)^{164}Hf$	+3.6
$^{181}Ta(\pi^-,16n)^{165}Hf$	+12.2
$^{181}Ta(\pi^-,15n)^{166}Hf$	+22.5
$^{181}Ta(\pi^-,13n)^{168}Hf$	+40.7

Figure captions

Fig. 1 : Experimental arrangement of the counter telescope and Ge(Li) detectors.

Fig. 2 : Prompt and delayed γ-ray spectra from pions stopped in a 7.04 g/cm^2 Ta target using the Compton-suppressed Ge(Li)-NaI(Tl) detector combination (low energy region).

Fig. 3 : As Fig. 2 but high energy region.

Fig. 4 : Prompt and delayed γ-ray spectra from pions stopped in a 3.45 g/cm^2 Bi target using a 15 cm^3 semi-planar Ge(Li) detector.

Fig. 5 : As Fig. 2 but with a 3.45 g/cm^2 Bi target (low energy region).

Fig. 6 : As Fig. 3 but with a 3.45 g/cm^2 Bi target (high energy region).

Fig. 7 : Yield of Pb (filled circles) and Tl (open squares) isotopes from pion capture reactions in Bi versus neutron multiplicity, x. The histograms represent calculations by Gadioli et al. [30] for reactions (π^-,xn), the dotted histogram, and $[\pi^-,p(x-1)n]$, the dashed one, in Au. The full line serves as a guide for the eye.

Fig. 8 : Yield of even Hf isotopes from pion capture reactions in Ta versus the neutron multiplicity, x. Note that the yield refers to the $4^+ \rightarrow 2^+$ transitions rather than the $2^+ \rightarrow 0^+$ ground state transitions. These latter all have energies of 80 to 100 keV and, owing to the rather high internal conversion coefficients ($\alpha_{tot} > 3$), they are hard to detect. The full line serves as a guide for the eye. The histograms represent calculations by Gadioli et al. [30], the dotted and dashed histograms are the calculated yields of Hf and Lu isotopes, respectively.

Fig. 9 : Yield of different members of the ground state rotational band in even Hf isotopes populated in the ^{181}Ta(π^-,xn) reaction.

Fig. 10 : The same data as in Fig. 9 now plotted versus the spin of the γ emitting level with the neutron multiplicity as a parameter.

Fig. 11 : The ratio of the population of high-spin states to that of low-spin states in even Hf isotopes versus x, the neutron multiplicity.

Fig. 12 : A simple illustration of possible mechanisms for the π^- absorption.
a) The pion is absorbed on a nucleon pair in the nuclear surface.
b) The pion is absorbed in the interior of the nucleus.

Fig. 13 : The experimental γ-ray yields of the $^{181}Ta(\pi^-,7n)^{174}Hf$ and $^{181}Ta(\pi^-,9n)^{172}Hf$ reactions versus the nuclear spin of the de-excited level. The dashed lines represent the calculated integral of the statistical angular momentum distribution for a $^{179}Hf(n,6n)^{174}Hf$ reaction before γ emission, using the optical model. Incident neutron energies used in the calculation presented in the figure are 50 and 70 MeV, respectively. The full line is the averaged yield over three energies in 10 MeV steps as explained in the text. The normalization to the experimental points is made for the $4^+ \rightarrow 2^+$ transitions.

Fig. 14 : The experimental γ-ray yields of some $^{209}Bi(\pi^-,xn)$ reactions versus the nuclear spin of the de-excited level. The full lines represent the calculated integral of the statistical angular momentum distribution for the $^{207}Pb(n,4n)^{204}Pb$ and $^{207}Pb(n,10n)^{198}Pb$ reactions before γ emission, as explained in the text. For the (n,4n) reaction we show the averaged yield for incident neutron energies between 50 and 70 MeV, for the (n,10n) reaction for energies between 80 and 100 MeV. The normalization to the experiment is made to the low-spin transitions.

Fig. 15 : The experimental γ-ray yields of the $^{209}Bi(\pi^-,5n)^{204}Pb$ reaction versus the nuclear spin of the de-excited level. The full lines represent the calculated integral of the statistical angular momentum distribution for the $^{207}Pb(n,4n)^{204}Pb$ and $^{207}Pb(n,10n)^{158}Pb$ reactions before γ emission, as explained in the text. The dashed lines represent the calculated yield for the $^{204}Hg(\alpha,3n)^{205}Pb$ reaction [32], which seems to be in better agreement with the data than the (n,xn) calculations. The dashed-dotted line serves as a guide for the eye.

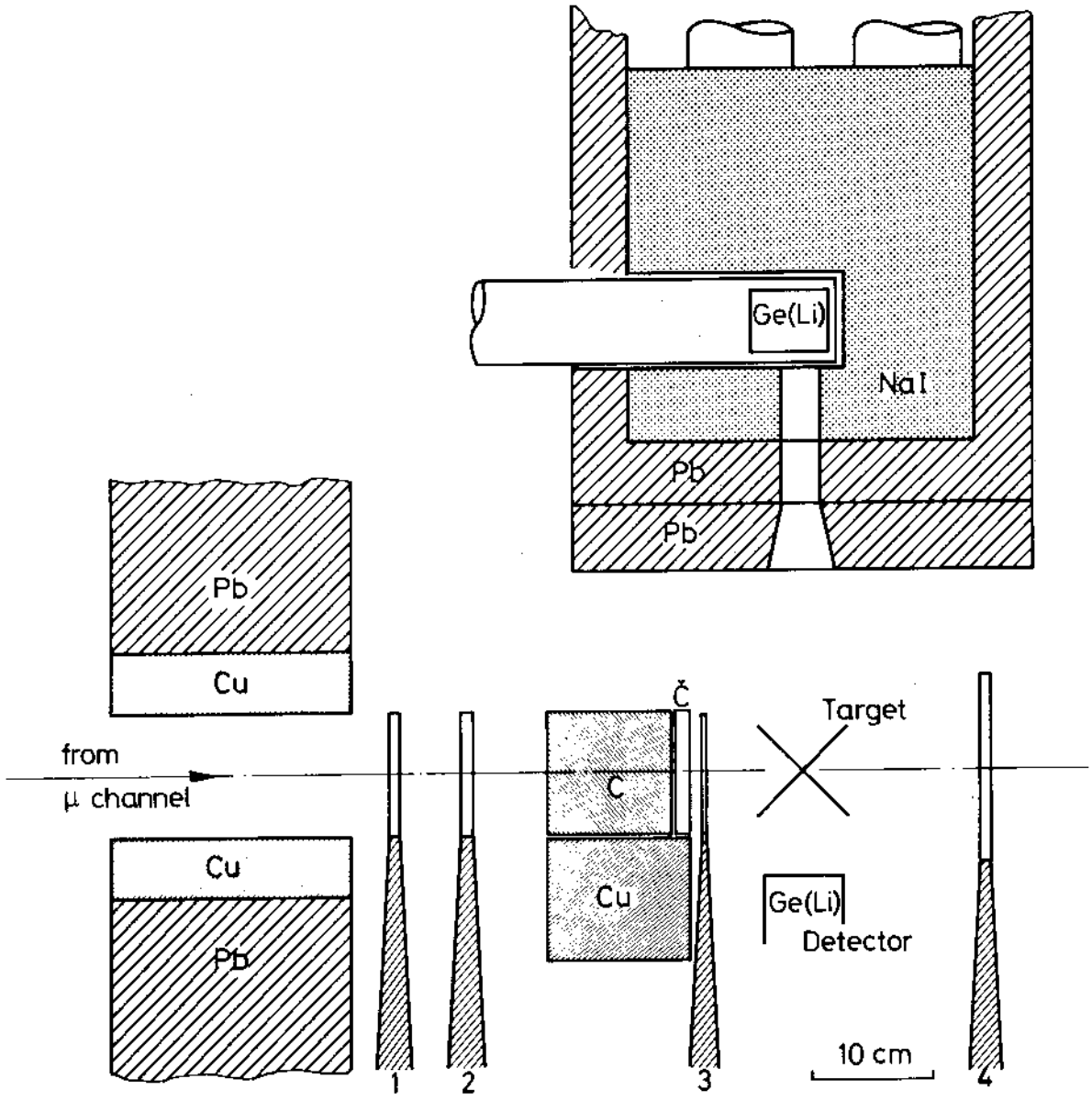
Ge(Li)
NaI
Pb
Pb
Pb
Cu
from
μ channel
Č
C
Cu
Target
Cu
Pb
Ge(Li)
Detector
10 cm
1
2
3
4

Fig. 1

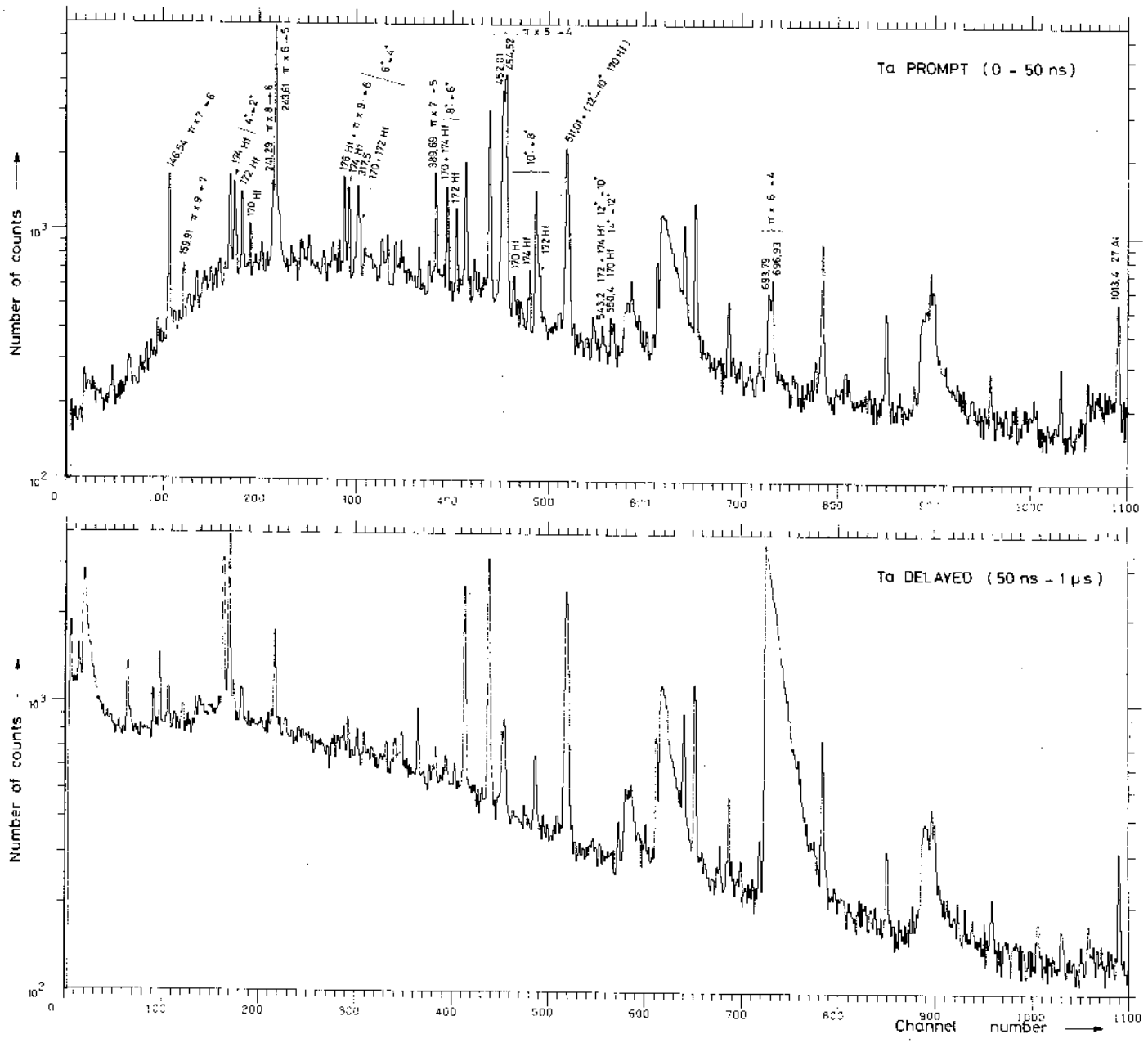
Ta PROMPT (0 - 50 ns)
Ta DELAYED (50 ns - 1 μs)
Number of counts
Channel number

Fig. 2

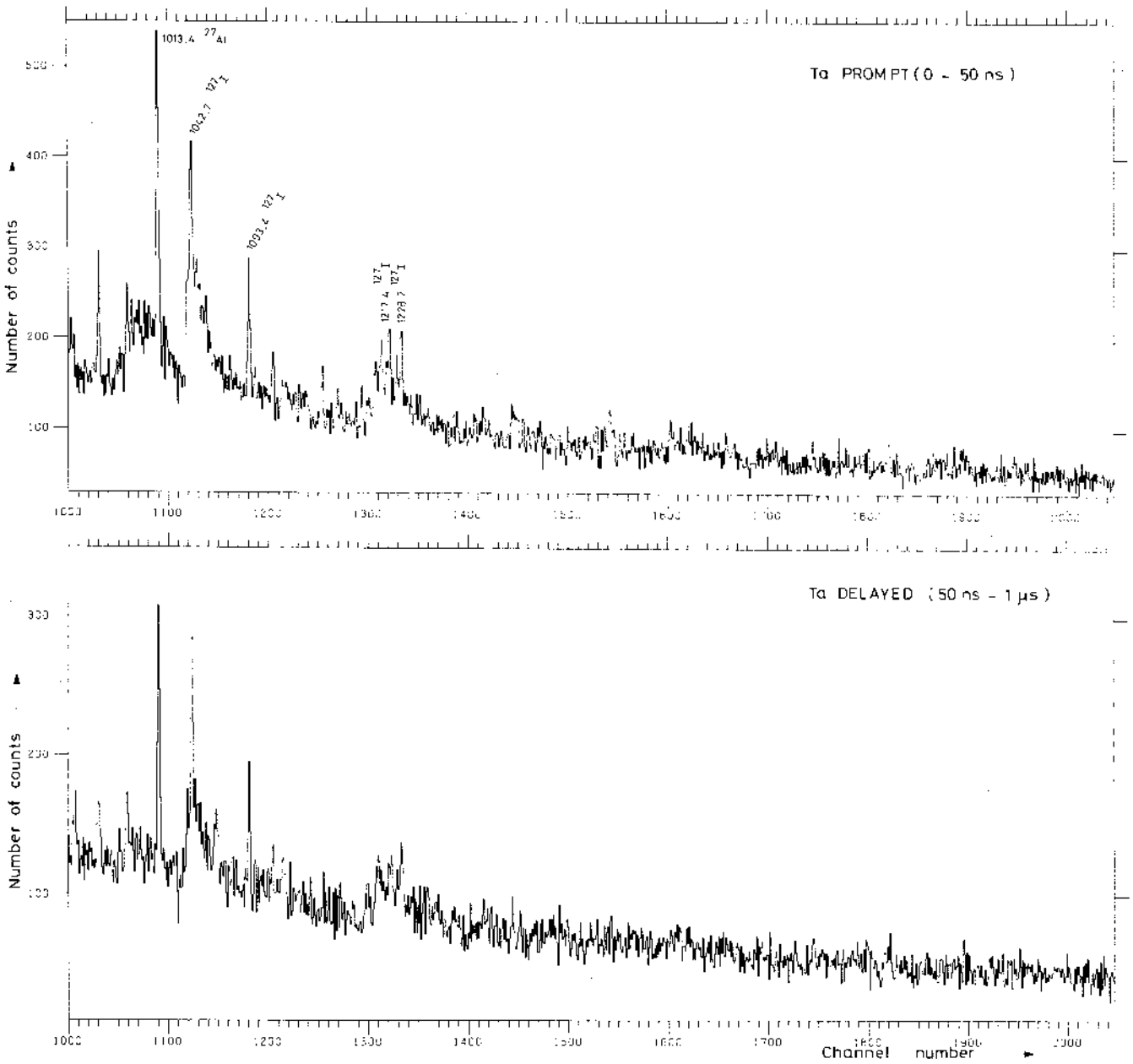
Ta PROMPT (0 - 50 ns)
Ta DELAYED (50 ns - 1 μs)
Number of counts
Number of counts
Channel number
1013.4 27Al
1042.7 127I
1093.4 127I
1271.4 127I
1298.7 127I

Fig. 3

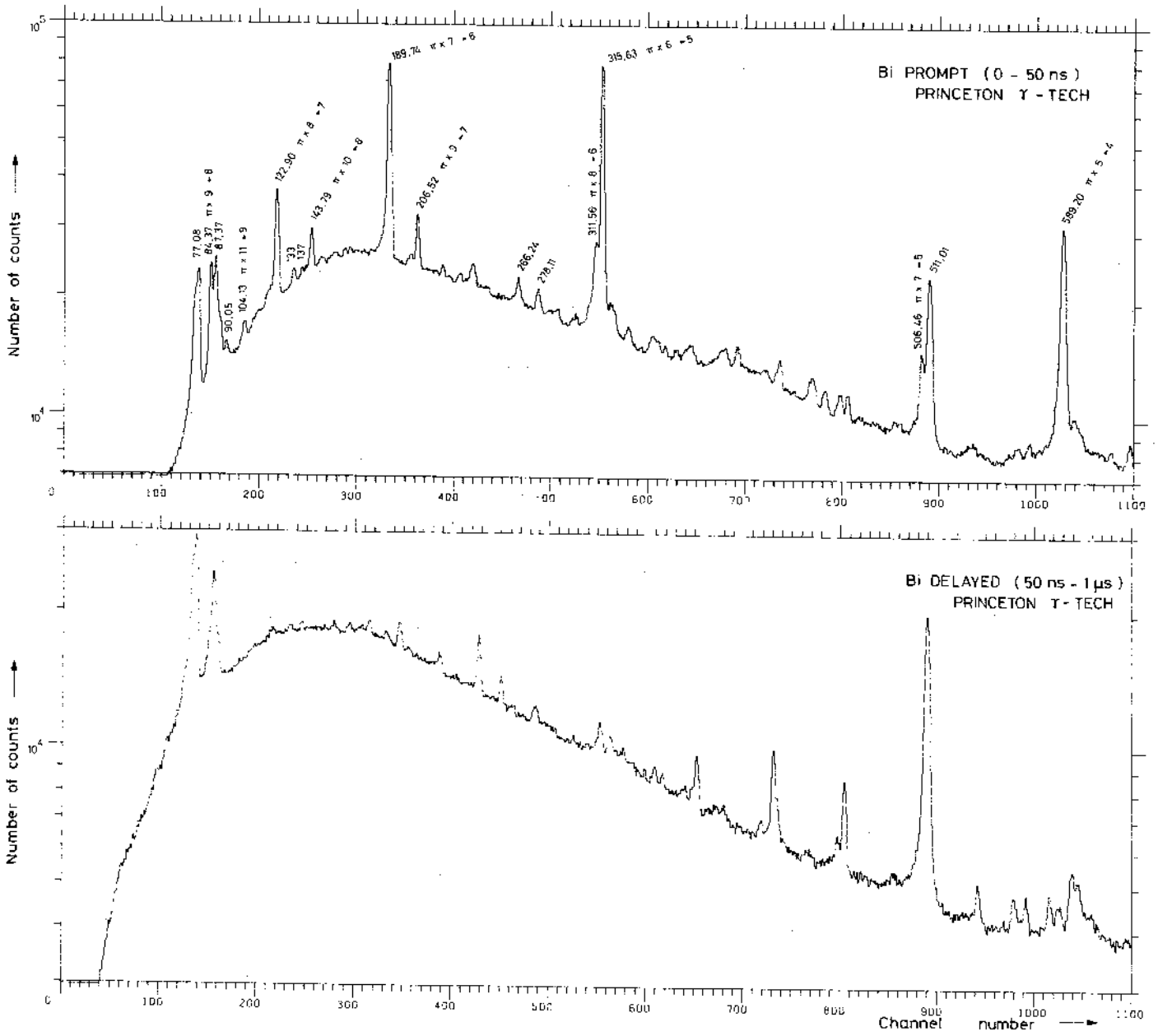
Bi PROMPT (0 - 50 ns)
PRINCETON γ - TECH
Number of counts
77.08
84.37
87.37
90.05
104.13
122.90
143.79
189.74
206.52
266.24
276.11
311.56
315.63
506.46
511.01
589.20
Bi DELAYED (50 ns - 1 μs)
PRINCETON γ - TECH
Number of counts
Channel number

Fig. 4

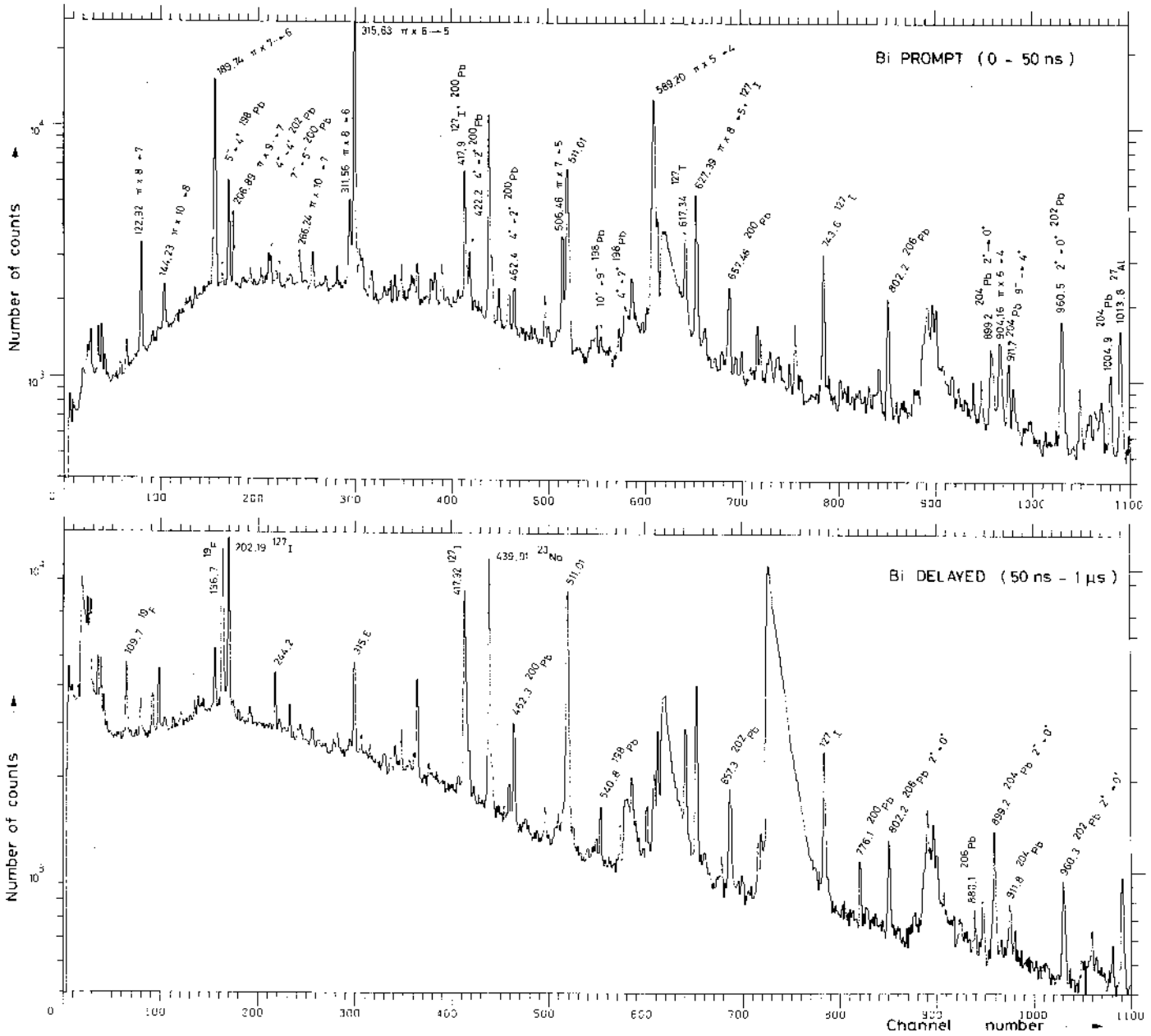
Bi PROMPT (0 - 50 ns)
Bi DELAYED (50 ns - 1 µs)
Number of counts
Channel number
315.63 π x 6 → 5
202.19 127I
438.91 23Na
511.01
417.92 127I
462.3 200Pb
657.3 202Pb
127I
776.1 200Pb
802.2 206Pb
899.2 204Pb 2+ → 0+
960.3 202Pb 2+ → 0+
1013.8 27Al

Fig. 5

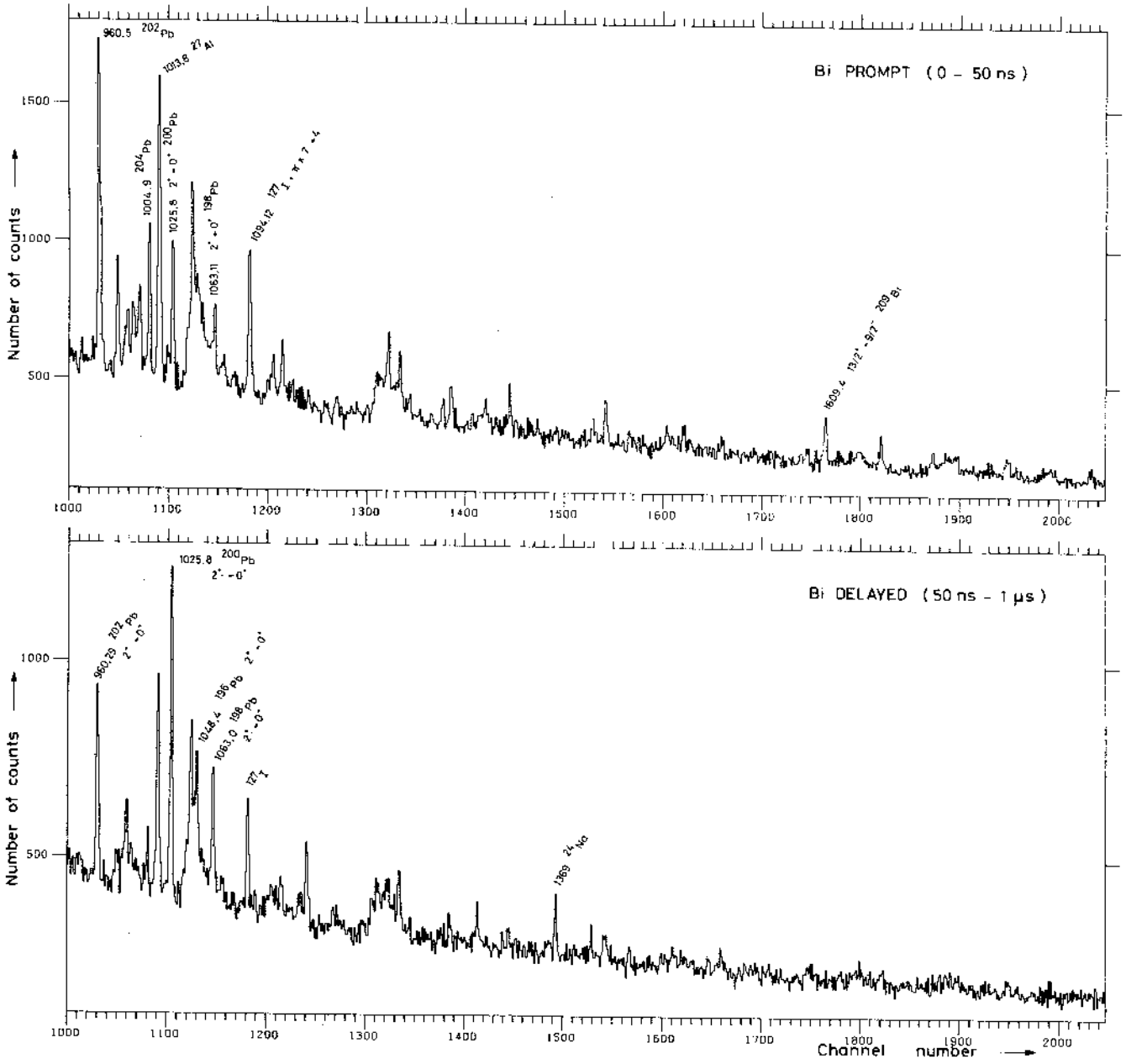
Bi PROMPT (0 - 50 ns)
Bi DELAYED (50 ns - 1 μs)
Number of counts
Channel number
960.5 202Pb
1013.8 27Al
1004.9 204Pb
1025.8 2+ - 0+ 200Pb
1063.11 2+ - 0+ 198Pb
1094.12 127I, π x 7 -4
1609.4 13/2+ - 9/2- 209Bi
960.29 202Pb 2+ - 0+
1025.8 200Pb 2+ - 0+
1048.4 196Pb 2+ - 0+
1063.0 198Pb 2+ - 0+
127I
1369 24Na

Fig. 6

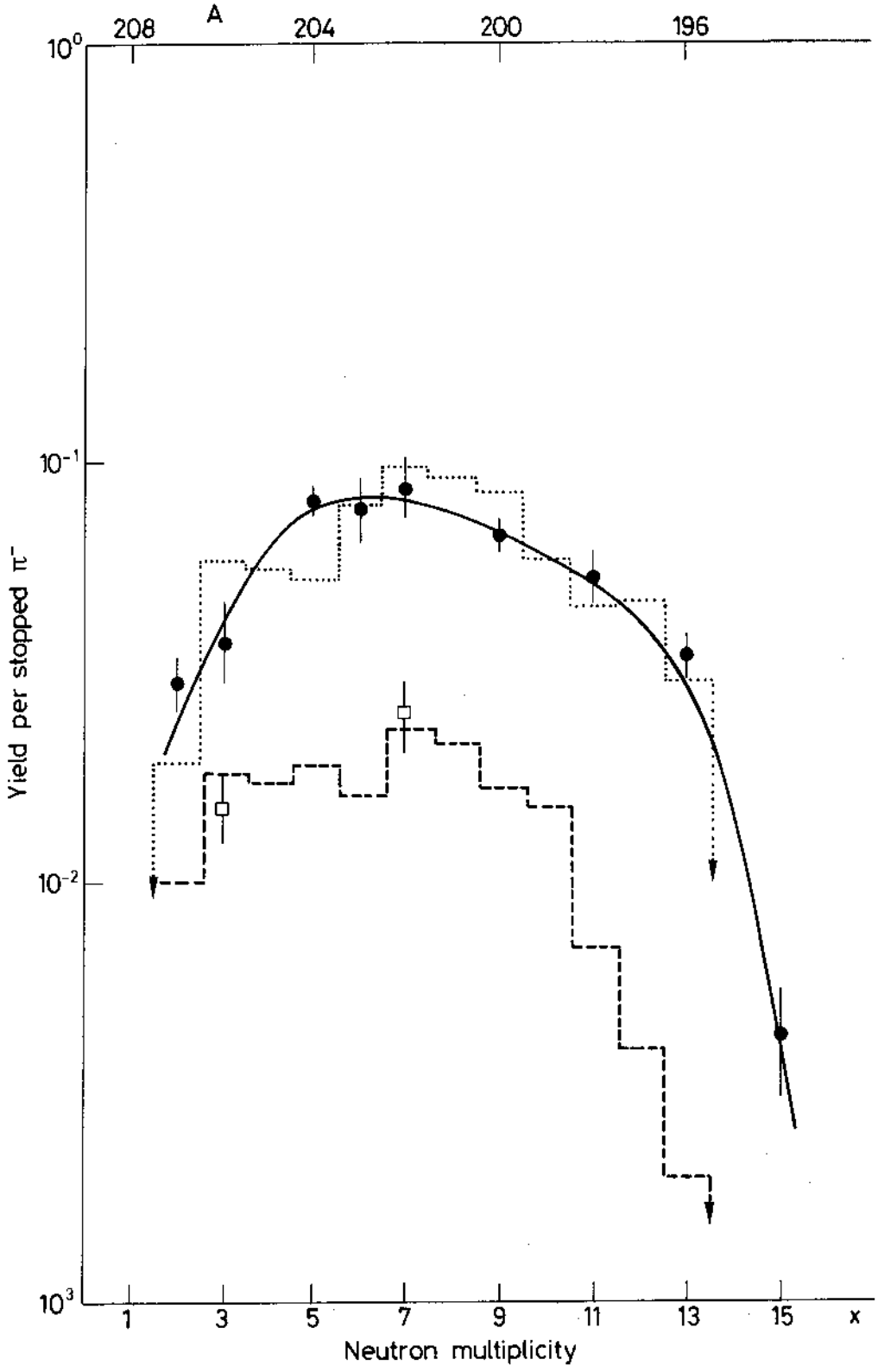
A
208
204
200
196
10^0
10^{-1}
10^{-2}
10^{-3}
Yield per stopped π^-
1
3
5
7
9
11
13
15
x
Neutron multiplicity

Fig. 7

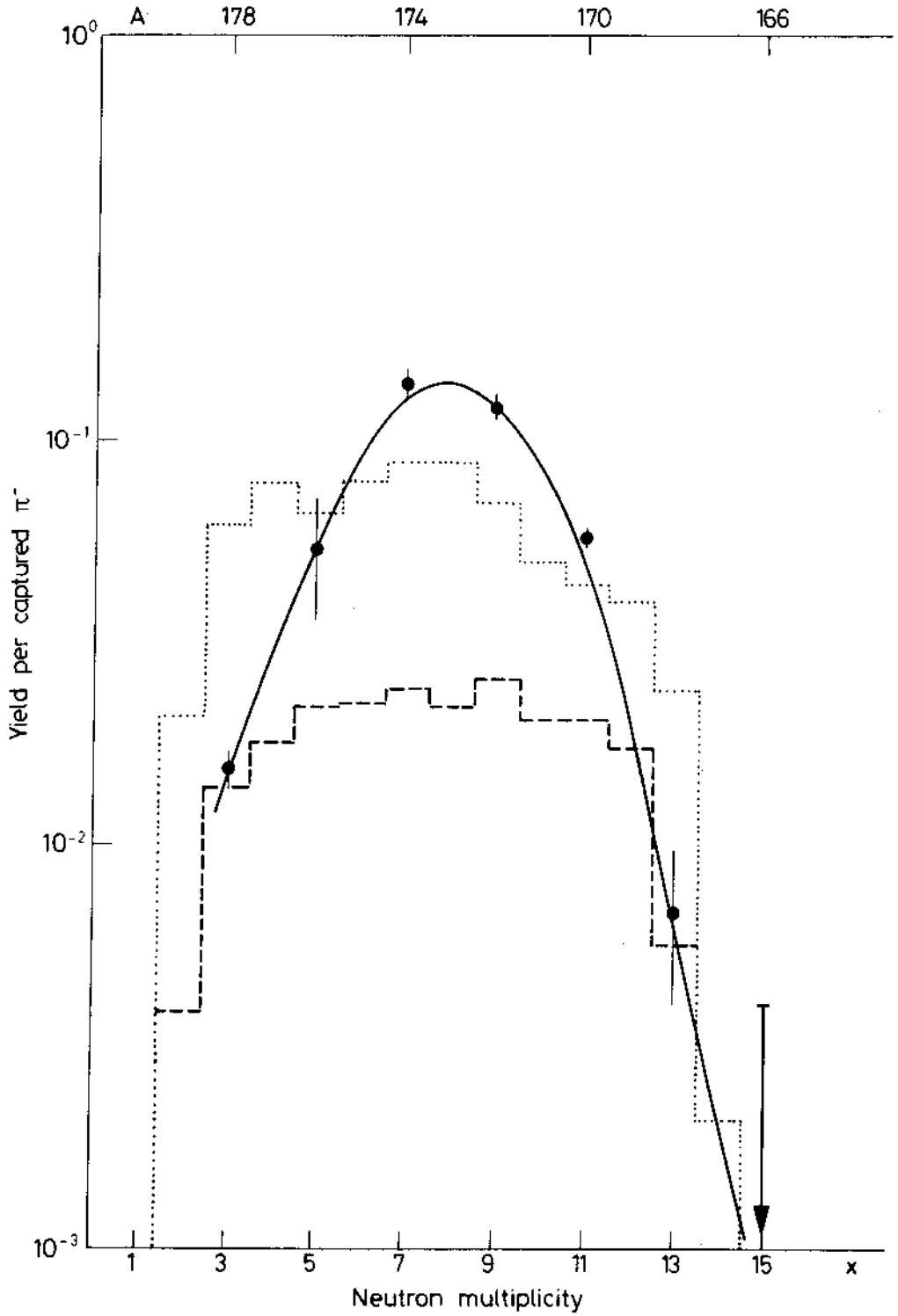
A
178
174
170
166
10^0
10^{-1}
10^{-2}
10^{-3}
Yield per captured π^-
1
3
5
7
9
11
13
15
x
Neutron multiplicity

Fig. 8

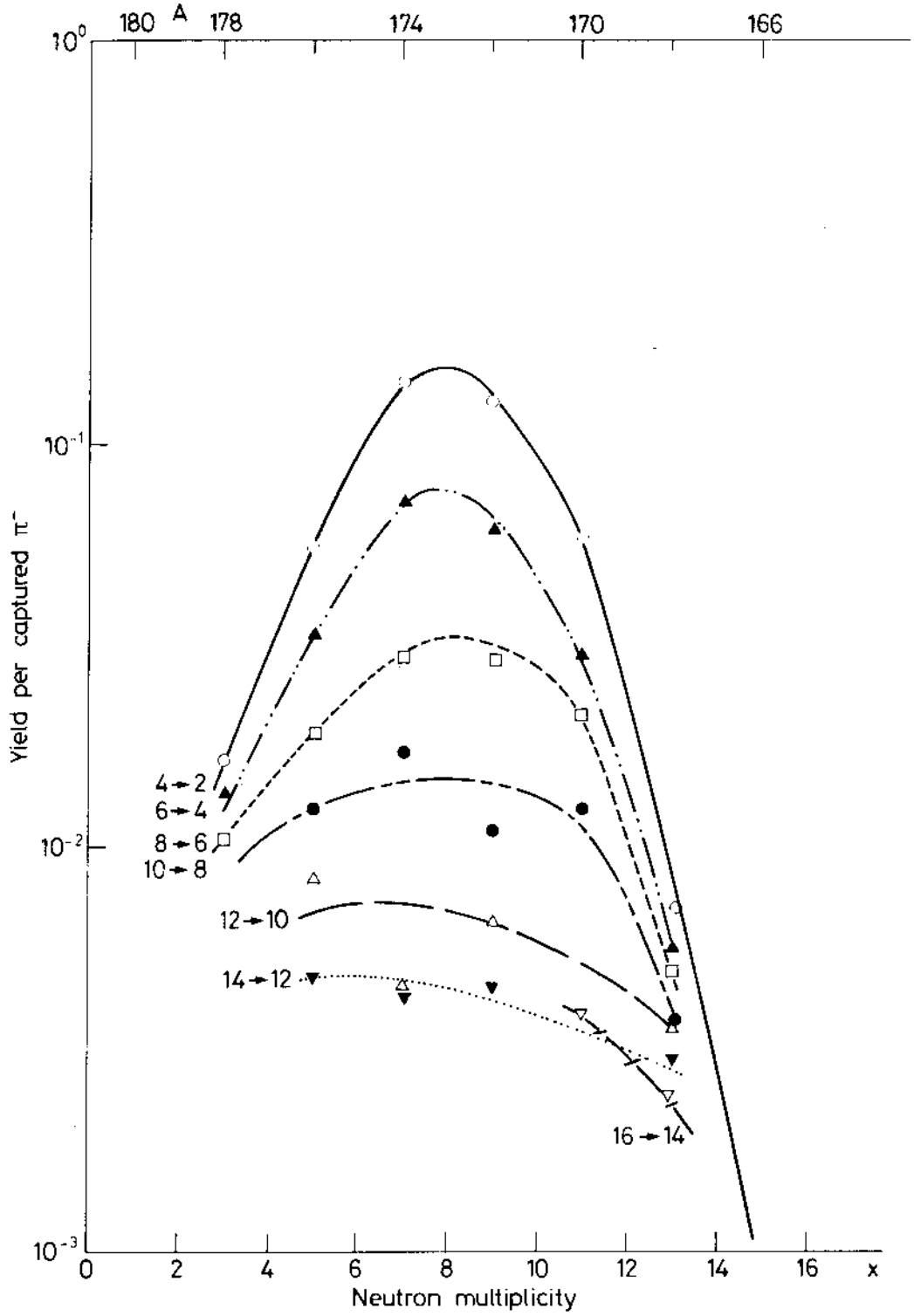
A
180
178
174
170
166
10^0
10^{-1}
10^{-2}
10^{-3}
Yield per captured π^-
4→2
6→4
8→6
10→8
12→10
14→12
16→14
0
2
4
6
8
10
12
14
16
x
Neutron multiplicity

Fig. 9

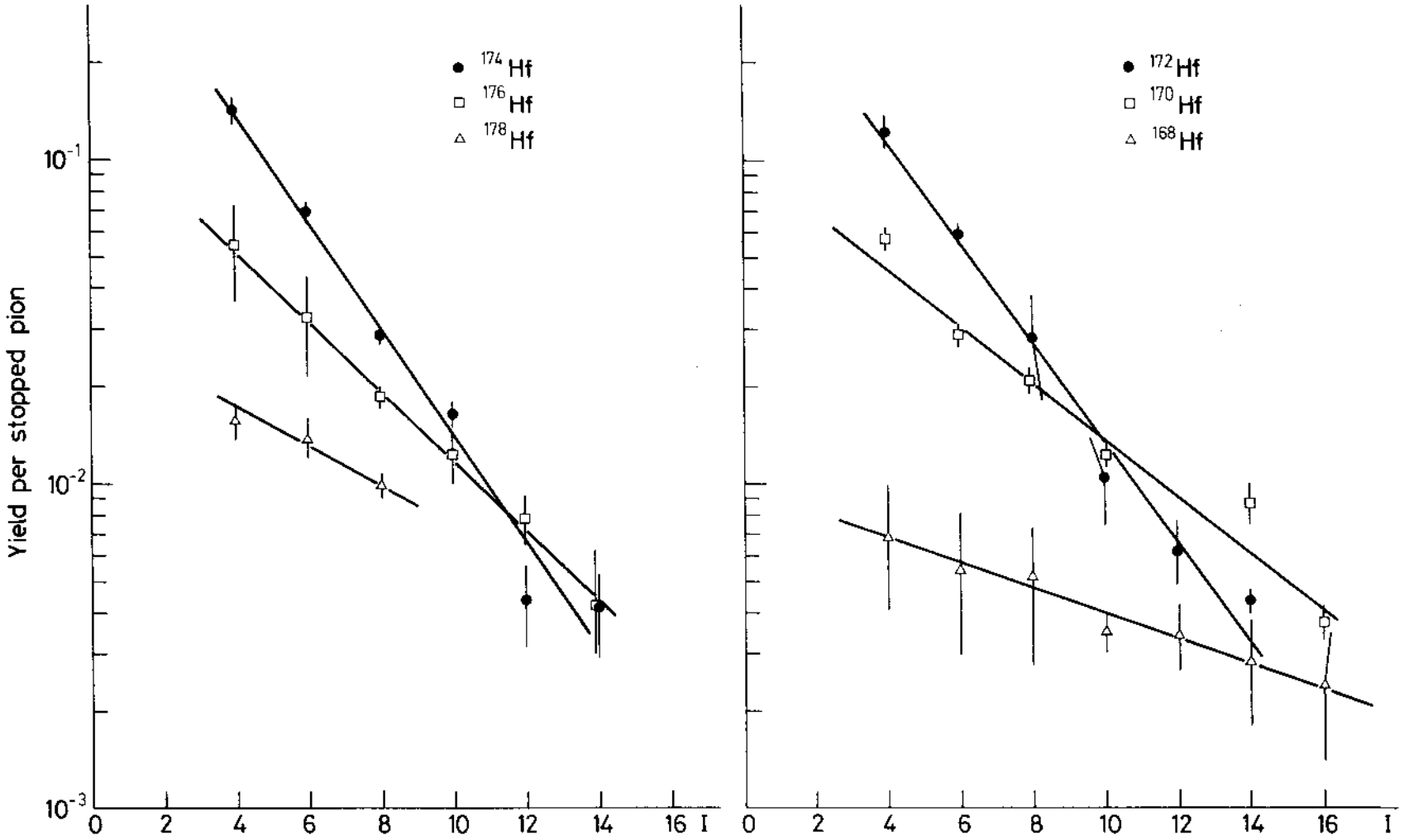
Yield per stopped pion
10^{-1}
10^{-2}
10^{-3}
0 2 4 6 8 10 12 14 16 I
^{174}Hf
^{176}Hf
^{178}Hf
^{172}Hf
^{170}Hf
^{168}Hf

Fig. 10

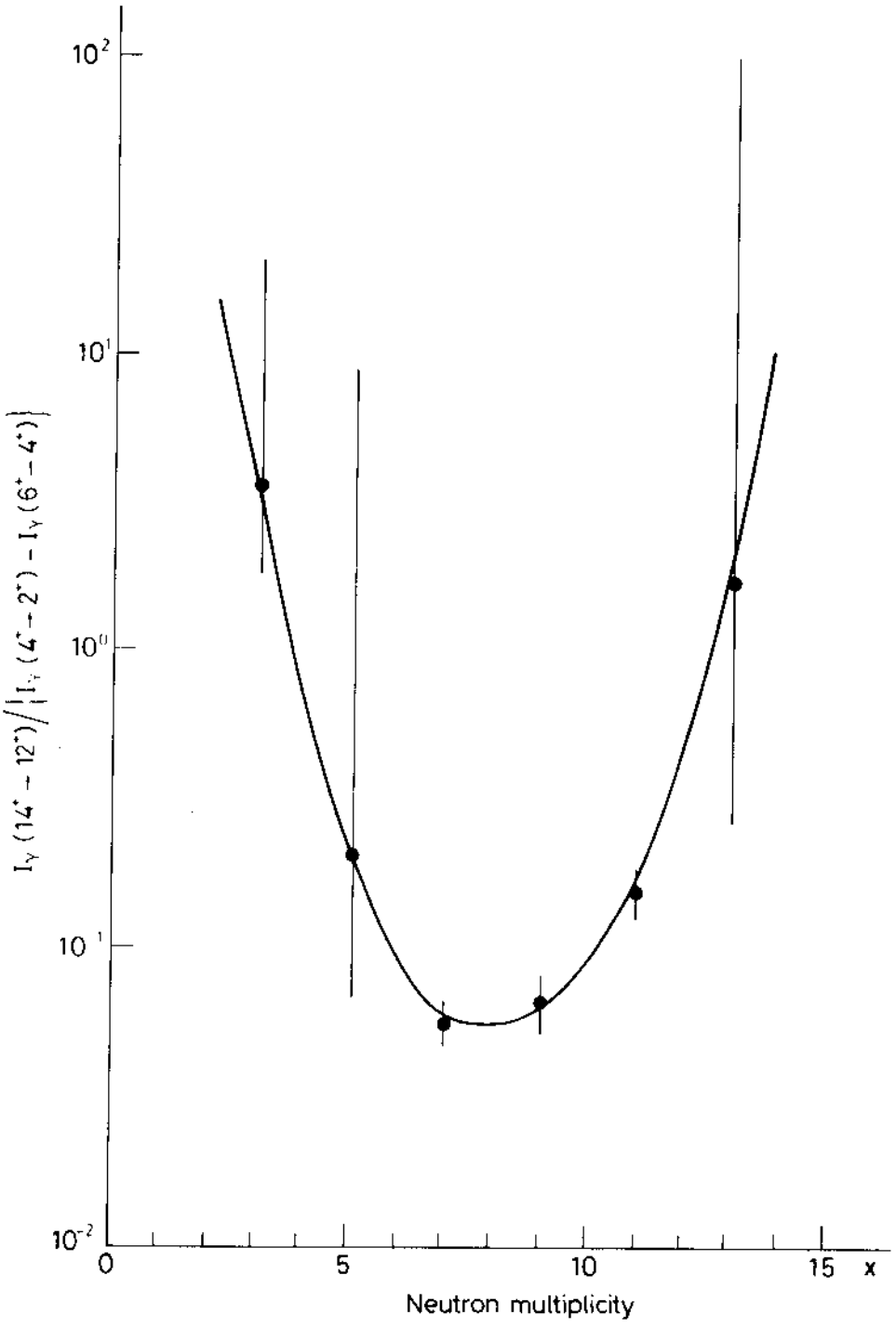
10^2
10^1
10^0
10^{-1}
10^{-2}
$I_\gamma(14^+ - 12^+)/\{I_\gamma(4^+ - 2^+) - I_\gamma(6^+ - 4^+)\}$
0
5
10
15
x
Neutron multiplicity

Fig. 11

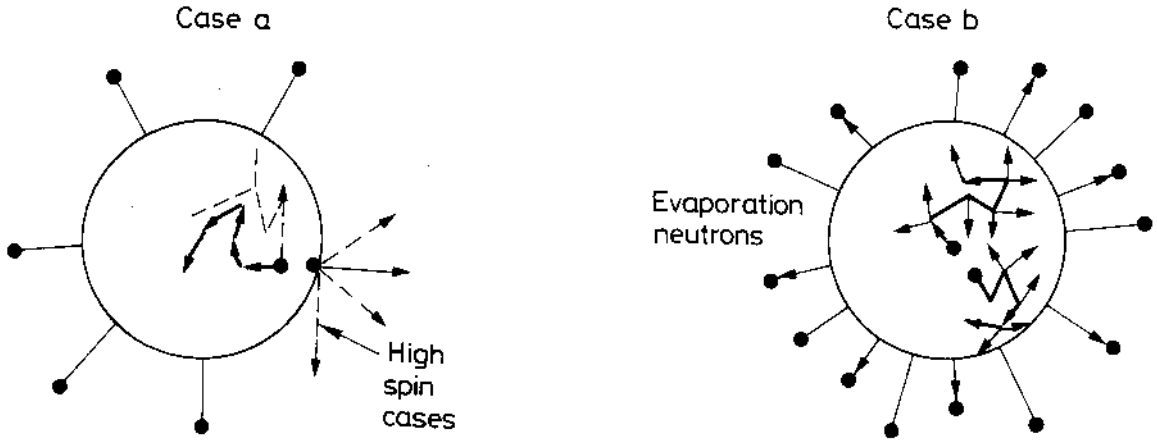
Case a
Case b
Evaporation
neutrons
High
spin
cases

Fig. 12

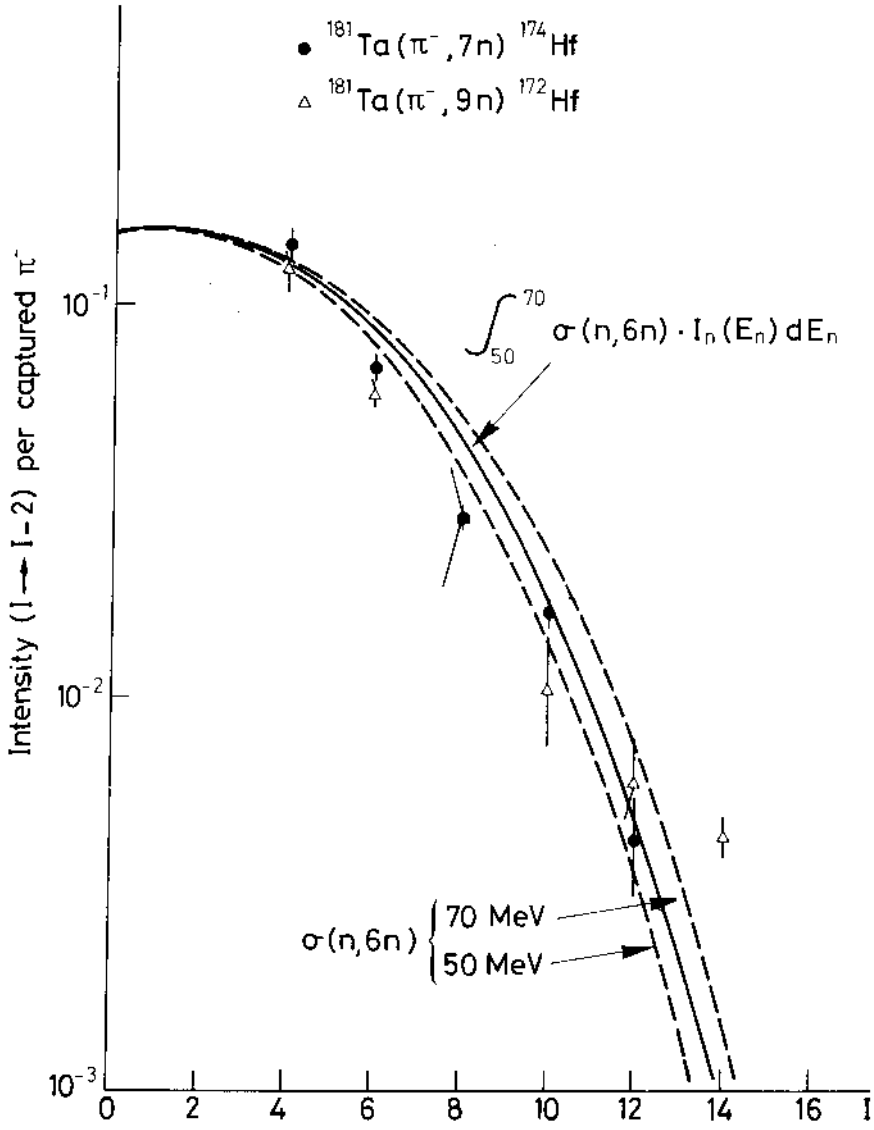
● $^{181}Ta(\pi^-, 7n)\ ^{174}Hf$
△ $^{181}Ta(\pi^-, 9n)\ ^{172}Hf$
$\int_{50}^{70} \sigma(n,6n) \cdot I_n(E_n)\, dE_n$
$\sigma(n,6n)$ 70 MeV
50 MeV
Intensity (I → I-2) per captured π^-
10^{-1}
10^{-2}
10^{-3}
0
2
4
6
8
10
12
14
16
I

Fig. 13

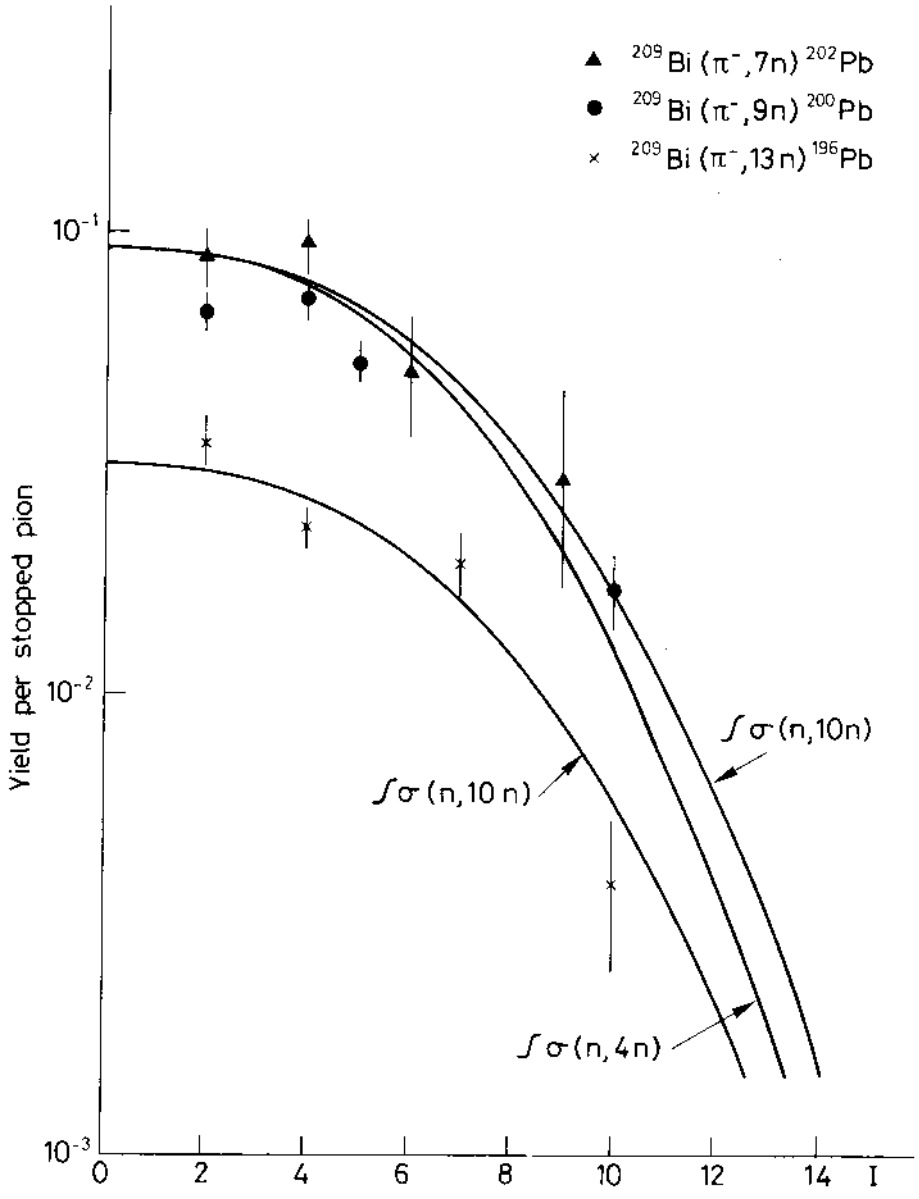
▲ ^{209}Bi (π^-,7n) ^{202}Pb
● ^{209}Bi (π^-,9n) ^{200}Pb
× ^{209}Bi (π^-,13n) ^{196}Pb
Yield per stopped pion
10^{-1}
10^{-2}
10^{-3}
0
2
4
6
8
10
12
14
I
$\int\sigma$(n,10n)
$\int\sigma$(n,10 n)
$\int\sigma$(n,4n)

Fig. 14

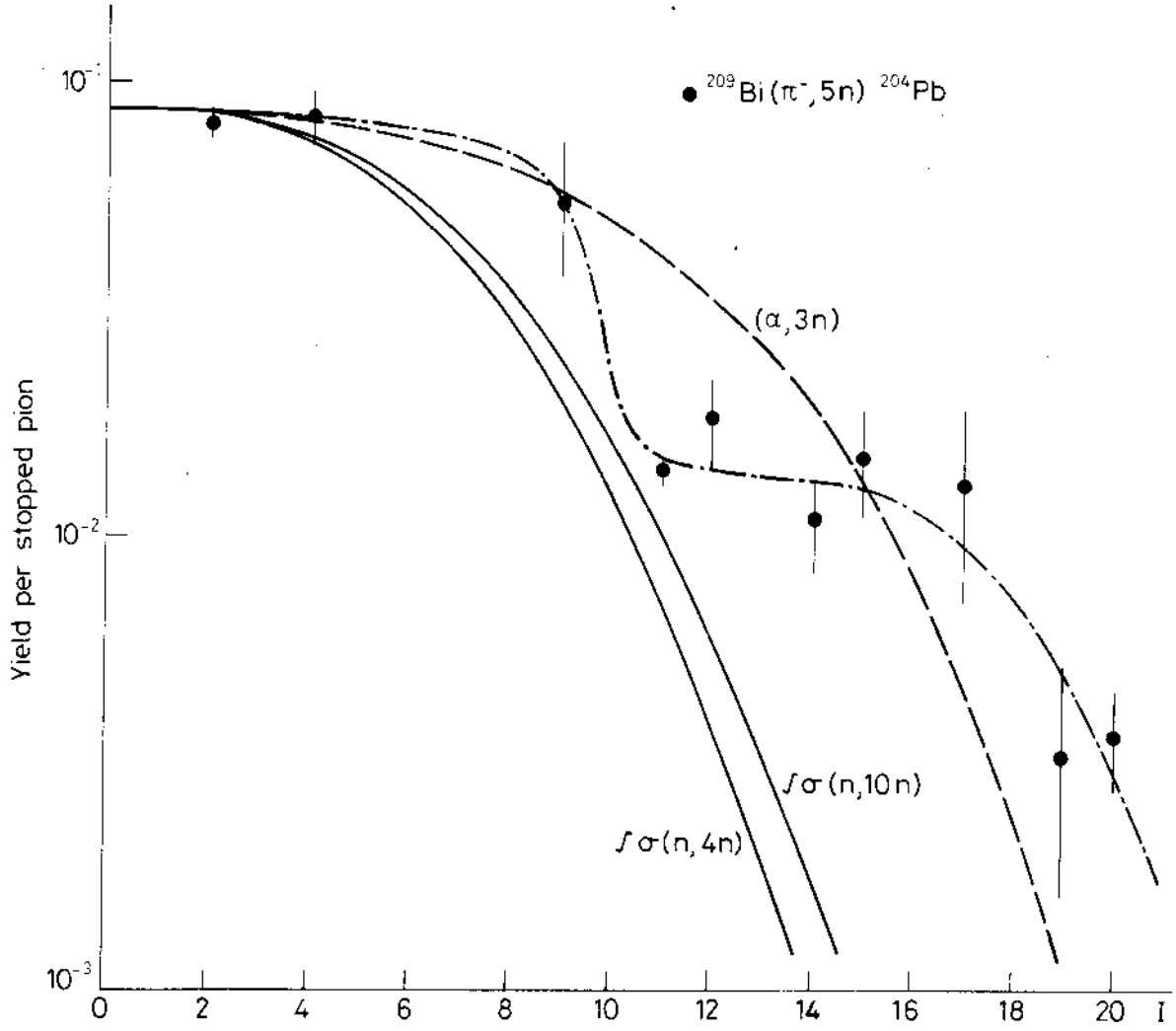
10^{-1}
10^{-2}
10^{-3}
Yield per stopped pion
● $^{209}Bi(\pi^-, 5n)\ ^{204}Pb$
$(\alpha, 3n)$
$\int\sigma(n, 10n)$
$\int\sigma(n, 4n)$
0
2
4
6
8
10
12
14
16
18
20
I

Fig. 15